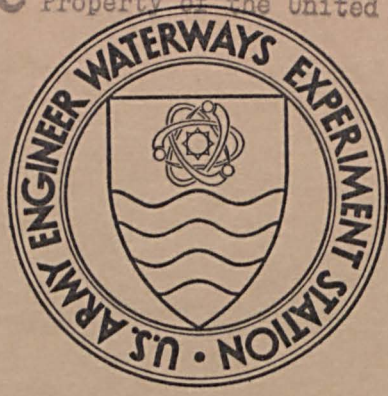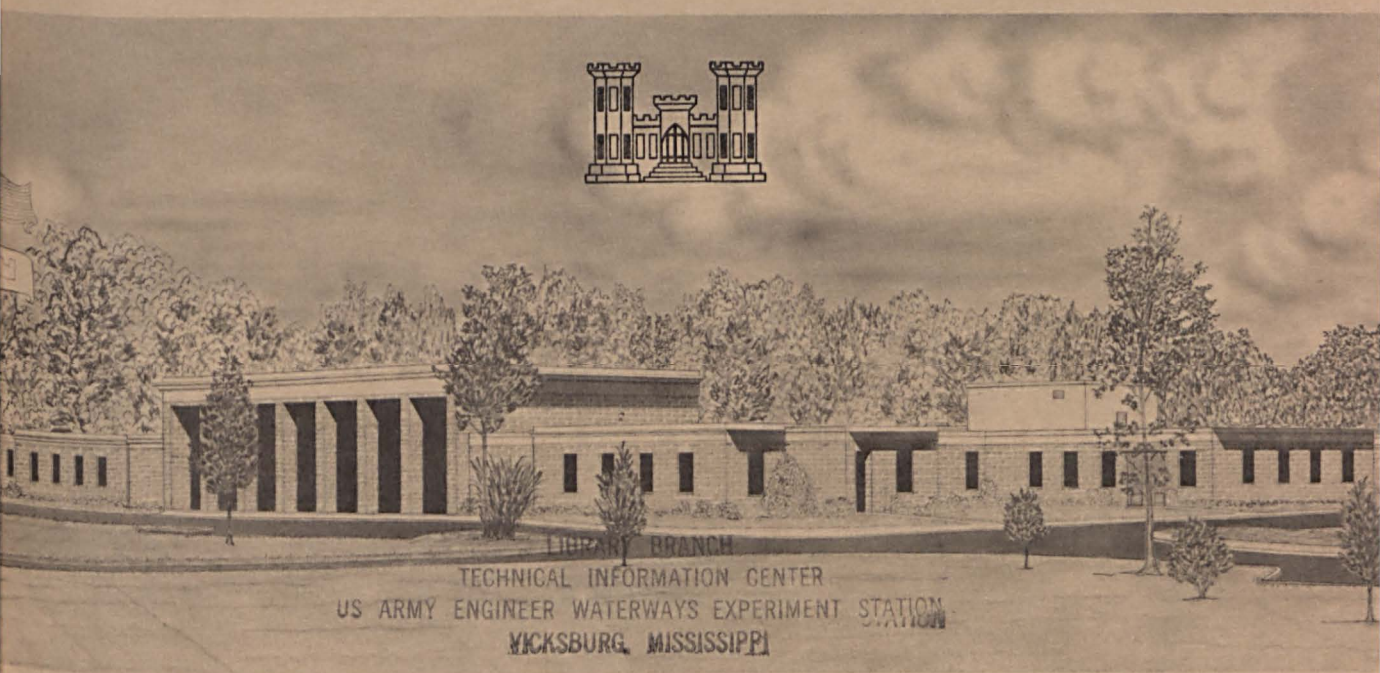MISCELLANEOUS PAPER C-73-12

PROPAGATION OF FAILURE IN A CIRCULAR CYLINDER OF ROCK SUBJECTED TO A COMPRESSIVE FORCE

by

R. L. Stowe

December 1973

PROPAGATION OF FAILURE IN A CIRCULAR CYLINDER OF ROCK SUBJECTED TO A COMPRESSIVE FORCE

by

R. L. Stowe

December 1973

ARMY-MRC VICKSBURG, MISS.

FOREWORD

The study reported herein was partly funded by Department of the Army Project 4A061101A91D, "In-House Laboratory Independent Research Program," Task 02, Work Unit 040, sponsored by the Assistant Secretary of the Army (R&D). The study was conducted during the period July 1970 to June 1973 in the Concrete Laboratory of the U. S. Army Engineer Waterways Experiment Station (WES) by Mr. R. L. Stowe.

Directors of WES during the conduct of the study and preparation of this report were BG E. D. Peixotto, CE, and COL G. H. Hilt, CE. Technical Director was Mr. F. R. Brown.

CONTENTS

LIST OF TABLES AND FIGURES

NOTATION

The following defines the major symbols used in this report.

Symbols

γ	Specific weight
C_o	Ultimate compressive strength
T	Tensile strength
S	Shear strength
ν	Poisson's ratio
E	Young's modulus of elasticity
G	Elastic shear modulus
L	Length
D	Diameter
D_p	Diameter of platen
D_s	Diameter of specimen
b	Base
h	Height
r	Radius
A	Total number of cracks at a percent C_o in a 1/2-in. square
B	Average number of cracks at no-load in a 1/2-in. square
CDS	Crack density scheme
$\bar{x}$	Average value
s	Standard deviation
R	Range of observed values

CONVERSION FACTORS, U. S. CUSTOMARY TO
METRIC (SI) UNITS OF MEASUREMENT

U. S. customary units of measurement used in this report can be converted to metric (SI) units as follows:

Multiply	By	To Obtain
inches	0.0254	metre (m)
inches^2	0.00064516	metre^2 (m^2)
pound-mass	0.04535924	kilogram (kg)
pound-force/inch^2 (psi)	0.006894757	megapascal (MPa)
pound-force/inch^2/sec (psi/s)	0.006894757	megapascal/second (MPa/s)
kip/inch^2 (ksi)	6.894757	megapascal
Fahrenheit degrees	5/9	Celsius or Kelvin degrees*

---

* To obtain Celsius (C) temperature readings from Fahrenheit (F) readings, use the following formula: C = 5/9 (F - 32). To obtain Kelvin (K) readings, use: K = 5/9 (F - 32) + 273.15.

SUMMARY

The study was conducted to gain a better understanding of the propagation of failure in an intact rock subjected to uniaxial compression, and to ascertain if a particular finite element code could predict the initiation and the propagation of failure. An elastic-elastoplastic finite element code, laboratory compressive tests, and petrographic techniques have been used to achieve this purpose.

The study consisted of two phases. In Phase I, a two-dimensional finite element code was used to predict the initiation and the propagation of failure in rock models tested in compression. The models had different length to diameter (L/D) ratios and different end platen diameter to specimen diameter ratios (D_p/D_s). The change in L/D and platen diameter was expected to show the effect of end restraint and possibly provide data on which recommendations for optimum platen diameters could be based.

In Phase II, cylindrical rock specimens with L/D = 2 were tested in uniaxial compression; the specimens had the same end platen configurations and the same elastic constants as were used in the finite element models. After testing, the specimens were then sawed into sections, and one section from each of the specimens was polished and then examined for crack density.

Results of nine finite element models and two laboratory models compare quite favorably, i.e., model simulation reasonably predicted the failure characteristics of an actual model (intact cylindrical rock specimen) tested in compression. The finite element and the laboratory models show that failure commences in the center of the model and propagates upward and outward. The extent to which the failure propagates is partially dependent upon D_p/D_s and upon the elastic mismatch between platen and specimen. The failure plane for L/D = 2 and D_p/D_s = 1 in the finite element model is comparable to the observed failure plane in a duplicate laboratory specimen. The finite element results and the laboratory test results suggest a minimum L/D = 2.5 and a $1 = D_p/D_s \leq 2$ be used for unconfined compression testing of cylindrical rock specimens; a D_p/D_s = 1 is preferred because of minimum end restraint.

I. INTRODUCTION

Opening Remarks

The propagation of failure in geologic materials is ill-defined; this is true for in-place materials as well as intact specimens. This circumstance arose out of necessity for tractable mathematics, and the subsequent use of empirical approaches and highly idealized phenomenological models. With the advent of high-speed computers and various numerical techniques, a more realistic assessment of the deformational behavior of geologic materials can be made. One approach to studying the deformational behavior of geologic materials is by the finite element method.

Numerous finite element codes are available and have been successfully used in order to ascertain a first approximation to a particular problem. Certainly there has been excellent correlation between data obtained with a simulated model and the actual model. Most of the early work has been done in the structural design fields; namely, those of aeronautical, architectural, and civil engineering. Relatively little work has been done in rock mechanics to determine whether or not model simulation can be used to predict the failure characteristics of geologic materials subjected to various states of stress. This is especially true of laboratory intact rock cores.

The present study was designed to contribute to an understanding of how well an intact rock can be modeled using a theoretical model and laboratory tests of the same model. An elastic-elastoplastic finite element code was used to analyze the failure growth of intact rock specimens subjected to uniaxial compression. Intact rock specimens

1

with the same dimensions, test configurations, and physical properties as the finite element model were tested in the laboratory and examined for failure zones and the propagation of failure. It should be noted that the techniques developed could be equally applicable to analysis of the behavior of more complex structures (e.g., underground mine openings).

Previous Studies

The theoretical aspects of how brittle materials fail have been extensively studied, and a number of failure theories have been proposed. However, it is generally considered that the Coulomb-Navier theory of failure describes rock failure quite adequately. The reason is that more requirements for failure of rock are satisfied; e.g.: (1) the theory does not assume the same behavior in compression and tension, (2) the theory includes a shear stress component, and (3) it accounts for increased shearing stress with some normal stress. Dahl's (1969) finite element code incorporates a generalized anisotropic version of Coulomb yield criteria.

Other investigators have studied both the failure mechanism and the propagation of failure in brittle materials subjected to compressive loads (Paulding, 1965; Brace and Bombolakis, 1963; Walsh, 1965; and Bieniawski, 1968). Certainly the mechanism by which a brittle material fails and the growth of the failed zone are interrelated. However, since this thesis is basically concerned with tracing the failure in a circular cylinder of intact rock subjected to compressive forces, previous investigations dealing with detecting the failure zone will be discussed. Several techniques could be used to detect these zones.

2

For brittle rocks tested in unconfined compression, it is generally accepted that failure initiates at or shortly before the transition between elastic and inelastic behavior. Normally, a competent rock will start to fail sometime after 80 percent of the ultimate compressive stress has been applied. Cook (1965) employed a technique which depicted this transition quite clearly. Shown in Figure 1 is the stress-strain curve and the envelope of microseismic activity for Tennessee marble loaded to fracture in compression. Both the stress-strain history and the microseismic-strain activity indicate failure starting at about 87 percent of the ultimate stress. Although this work does not trace failure zones, it does strongly indicate at what stress level failure zones develop.

Hardy and others (1968 and 1969) and Chugh (1968) have investigated microseismic activity in relation to the inelastic behavior in geologic materials under stress. These investigators show increased microseismic activity with increased stress levels: Hardy and others (1969) in the compression mode, while Chugh (1968) in the tension mode of testing. Chugh (1968) suggests that techniques should be developed to monitor microseismims as close to their source as possible.

Scholz (1968) has developed an excellent technique whereby he employs a multitransducer array to locate in space the largest microfracture events of rock tested in compression. For a particular granite, Scholz observed a rapid acceleration of microfracturing activity at about 92 percent of the fracture stress. At stresses above this level of accelerated activity, marked clusters of microfractures on the eventual fault plane were recorded (see Figure 2). This work suggests that the place of fracture initiation and possibly the

3
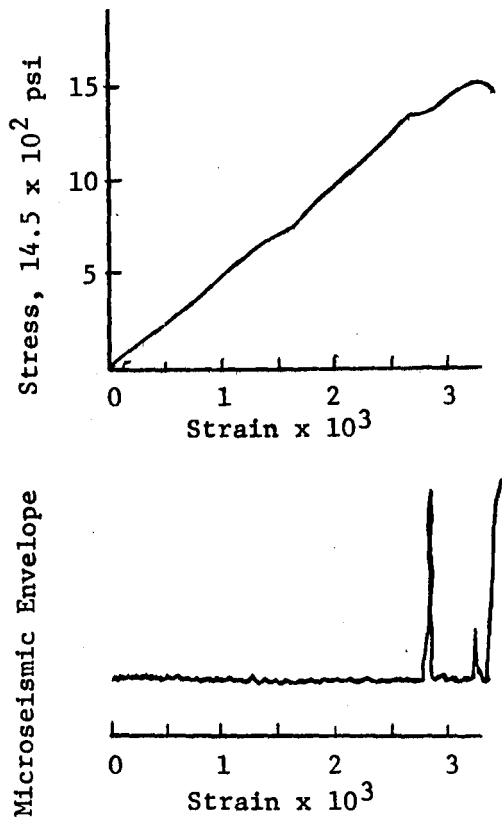
Figure 1. Stress-Strain Characteristics and the Envelope of Microseismic Activity for a Specimen of Tennessee Marble Loaded to Fracture in Compression (After Cook (1965)).

4
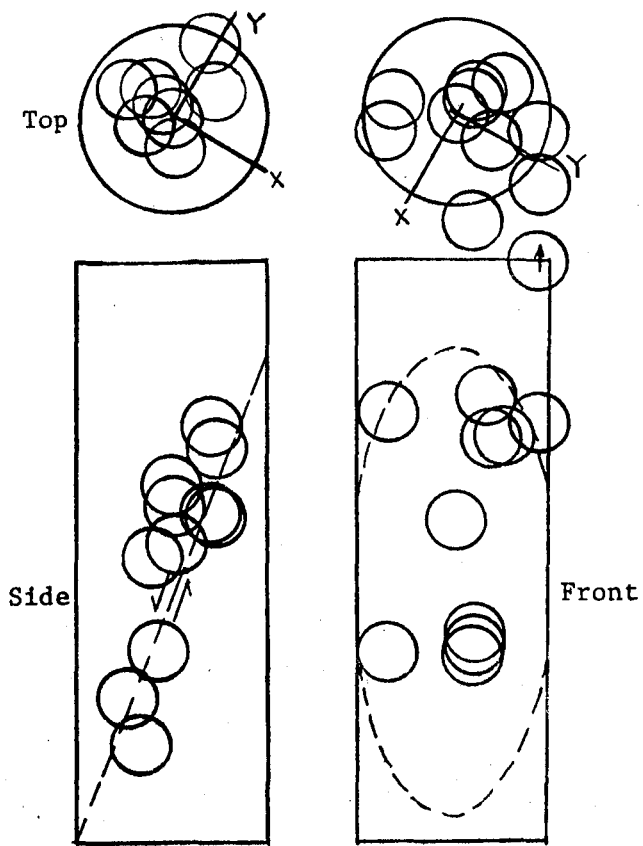
Figure 2. Marked Clusters of Microfractures on the Eventual
Fault Plane on a Specimen Loaded Under Compression
as Detected by Microseismic Techniques (After Scholz).

propagation of failure could have been predicted. Microseismic activity has a potential use, then, for determining the propagation of failure in rock tested in compression.

Other techniques, such as the penetrating die technique and microscopic examination of the failure zones, have been successfully used. The penetrating die technique has been used by Hsu and others (1963) to determine the quantity and orientation of cracks in concrete. Stowe (1967) has employed the same approach for ascertaining crack density (a measure of fracturing) in grouts subjected to statically and rapidly applied compressive loads.

Probably one of the most direct techniques used to show the initiation and the propagation of failure in specimens under uniaxial compression was utilized by Hawkes and Mellor (1970). These investigators subjected ice (which may actually be classed as a polycrystalline geologic material) to compressive loads and recorded on film the development of failure zones and the growth of these zones. They stated that the mode of failure in which the ice crumbles by internal cracking and then is burst apart by conical or wedge-shaped end segments was representative of the observed behavior of most rocks. However, they recognized that the mode of failure in the ice was definitely influenced by end constraint imposed by the loading platens and not necessarily intrinsic material properties.

Studies involving direct observation of the rock structure combined with theoretical prediction of the location of failure initiation and propagation have been limited. The work of Peng and Johnson (1972) is probably most closely related to the present study. In the investigation they employed a theoretical analysis of stress and strain to

determine stress concentrations within cylindrical specimens of Chelmsford granite subjected to various end-boundary conditions. Then, after compression tests, an eight-power binocular microscope was used to ascertain the crack density on a longitudinal surface cut from laboratory-tested specimens. The specimens had been loaded to various increments of the ultimate compressive strength.

It is important to note that several differences exist between Peng and Johnson's investigation and the present study. First, their theoretical solutions for stresses within a cylinder subjected to compressive loads were based upon elastic theory; therefore, they were unable to show the initiation and propagation of failure in their theoretical model. By using contour maps of stress concentrations within specimens, they could only indicate areas where failure might initiate. Second, using specimens with $L/D = 2$, where $D = 1.64$ in., these investigators examined thirty-two 0.41-in. squares from which they determined a crack density; in other words, the total number of cracks per 0.17 in.^{2} The method is certainly a valid one for determining gross crack densities; however, in the present study, it will be shown that a 0.17 in.^{2} area appears too large to allow the propagation of failure to be ascertained with a high degree of confidence.

Purpose and Scope

The purpose of the present study has been to obtain some understanding of the propagation of failure in an intact rock subjected to uniaxial compression, and to ascertain if a particular finite element code could predict the initiation and the propagation of failure. An elastic-elastoplastic finite element code, laboratory compressive tests, and petrographic techniques have been used to achieve this purpose.

The study consisted of two phases. In Phase I, a two-dimensional finite element code was used to predict the initiation and the propagation of failure in rock models tested in compression. The models had different length to diameter (L/D) ratios and different end platen diameters. The change in L/D and platen diameter was expected to show the effect of end restraint and possibly provide data on which recommendations for optimum platen diameters could be based. The analysis of the models consisted of determining stress trajectories and depicting the progression of yielded elements.

In Phase II, rock specimens with L/D = 2 were tested in uniaxial compression; the specimens had the same end platen configurations and the same elastic constants as were used in the finite element models. After testing, the specimens were then sawed into sections, and one section from each of the specimens was polished and then examined for crack density. Unloaded specimens were also examined for crack density. An apparatus used for determining air-void content in concrete was used to examine the polished sections.

II. FINITE ELEMENT PROCEDURE

General Description of the Finite Element Method

Detailed descriptions of the finite element method (Argyris, 1960; Clough, 1960; and Zienkiewicz and Cheung, 1967) have been given elsewhere. A brief description of the method will be presented here.

In the finite element method, a body is represented by an assemblage of discrete units called finite elements. The elements are interconnected at specific points called nodes or nodal points; it is the location of the nodes in space which defines the size and shape of a body. Suitable displacement functions are assumed for defining displacements over each element; the unknown quantities of the functions are the displacements of the nodes. Quite suitable displacement functions are polynomial or trigonometric functions, and because of ease of mathematical manipulation, polynomials are commonly used in the finite element method.

The principle of potential energy is normally used to formulate equilibrium equations for each element. Equilibrium equations for the body are then obtained by combining the equations for the individual elements. These equations are altered to accommodate displacement boundary conditions and then solved to determine the unknown nodal displacements. If it is desirable to have the strains or stresses rather than displacements, additional computations can be performed.

Finite Element Code

Dahl's (1969) finite element code appeared to be suitable for the type of problem presented in this study. Among other parameters, Dahl's code accounts for the deformation characteristics of an elastic-elastoplastic material. The post-yield behavior for this type of

material is partially represented by constrained plastic flow and partially by elastic deformation. The code is applicable to two-dimensional plane strain problems. Although the uniaxial compression test is not a plane strain problem, it is believed that the code can be used to indicate when and where yielding in the model occurs. Those fabric elements that lie on the surface of the central plane of a circular specimen tested in uniaxial compression (the plane of the saw cut across a diameter of the specimen) are assumed to be in a plane-strain condition.

The code indicates at what load level the first element has yielded; e.g., when the material of an element has become plastic. From the initial yield load level to the final load level, an incremental loading path is followed, and at each load increment all other elements in the model are checked for yielding. The yielded elements with corresponding stress, strain, and displacement for each load increment are printed out. With this information, yielding within the model can be traced.

The elastic fundamental properties, E and ν, and the mechanical properties C_o and T, which were input code parameters, were obtained from laboratory tests; these tests will be described in Part III. The input values G and S were calculated using the above-mentioned properties; that is:

$$G = \frac{E}{2(1+\nu)} \tag{1}$$

where G is the shear modulus, E is Young's modulus of elasticity, and ν is Poisson's ratio; and

$$S = \frac{C_o \times T}{C_o + T} \tag{2}$$

where S is the shear strength, C_o is the ultimate compressive
strength, and T is the tensile strength (equations (1) and (2) from
Dahl, 1969). The equations used to calculate G and S assume
isotropy and a linear yield envelope, respectively. Actual material
properties used in the code are given in Table 1.

Finite Element Model

     The finite element model was constructed after consideration of
the more commonly used test configuration for uniaxial compression test-
ing. Numerous rock mechanics laboratories in this country comply with
the ASTM Standard Method of Test for Compressive Strength (ASTM 1971).
The method allows for the length-to-diameter ratio (L/D) of 2.0 to 2.5
and a diameter of not less than NX core size (approximately 2-1/8 in.).
The modeled specimen diameter in this study is 2 in. It further allows
that the platen shall be at least as large as that of the test specimen
but shall not exceed twice the diameter of the test specimen. In other
words, the ratio of the diameter of the platen to the diameter of the
test specimen (D_p/D_s) shall be $1 \leq D_p/D_s \leq 2$. These latter specifica-
tions were complied with in only four of the nine models run in this
present study. Five runs were made to see what effect L/D = 3 and
D_p/D_s = 3 would have upon the load level at which failure initiated
and upon the propagation of failure. These results were compared with
the results obtained with the accepted test configurations.

     Figure 3 illustrates the composite finite element mesh used. Due
to symmetry, only one quarter of the test configuration was considered.
The composite model was composed of 120 elements and 77 nodes. Tri-
angular elements were used which had base (b) to height (h) ratios of
2 (b/h = 2) for the rock and b/h = 1 for the top two rows of elements

11

TABLE 1

Mechanical Properties Used in Finite Element Studies

E (ksi)	ν	G (ksi)	C_o (ksi)	T (ksi)	S (ksi)
		Rock Properties*			
8,650	0.26	3,433	21	0.815	0.784
		Steel Properties			
30,000	0.30	11,540	40	40	20

* Average values of E, ν, C, and T were taken from Saucier and Ainsworth (1971). Their data are described in more detail in Chapter III.
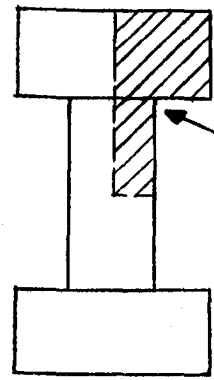
Figure 3. Finite Element Mesh Showing the Platen-Specimen
Configuration and the Geometry Used in the Different
Problems and Cases Investigated.

13

in the end platen. However, three separate problems having L/D of 2, 2.5, and 3 and three separate cases having D_p/D_s of 1, 2, and 3 were incorporated into the model. Each problem was run three times using one of the three cases per run for a total of nine runs. After Problem 3 was run with Case 3 (L/D = 3; D_p/D_s = 3), appropriate elements were subtracted from the composite model until all n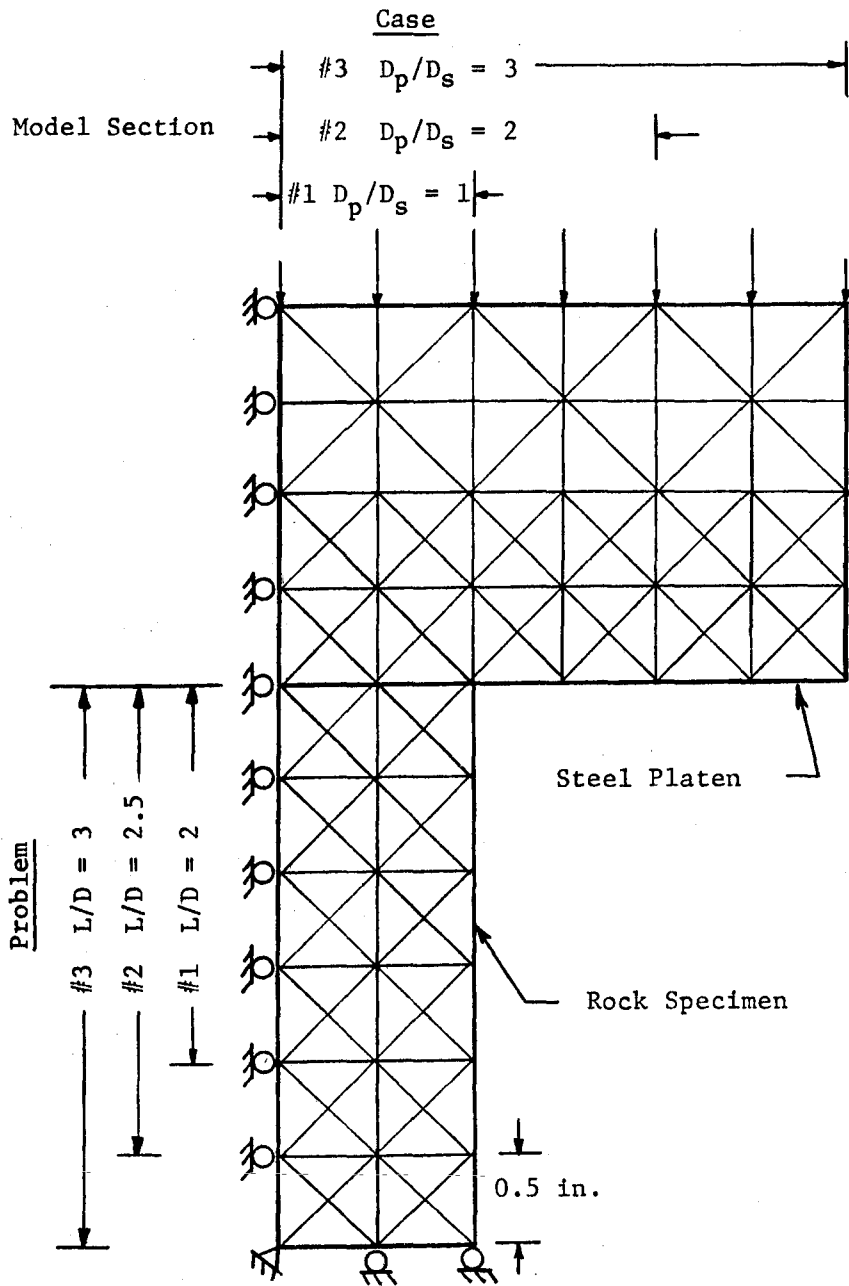ine runs were completed. The end platen thickness (2 in.) and the specimen diameter (2 in.) remained constant for all runs.

Steel end platens were used in the model and in the laboratory tests. It is recognized that an elastic mismatch results between the end platens and the specimen and that this mismatch will cause a non-uniform distribution of stress and strain throughout the specimen. The degree of nonuniform stress and strain is dependent both on the magnitude of the elastic mismatch and on any relative movement between the specimen and the end platens. For uniaxial compression tests where steel end platens are used, the specimen generally expands radially more than the end platens; e.g.:

$$\frac{\nu_s}{E_s} > \frac{\nu_p}{E_p} \tag{3}$$

where the subscripts s and p refer to the specimen and end platen, respectively. Frictional restraint is the outcome of this elastic mismatch, and the restraint causes shearing stresses to develop at the platen-specimen interface. A clamping effect is thus produced which causes a nonuniform state of multiaxial stress throughout the specimen. Admittedly, this is an unfavorable condition when so-called "true" rock properties are desired; however, since the above condition does exist in real life, it was incorporated in the present study.

The mechanical properties used as model input data in the finite element studies are given in Table 1. The rock properties listed are average values determined from uniaxial compression tests conducted in the laboratory, while the properties of the steel were obtained from the literature (Layne, 1969). The average compressive strength of the rock was used to calculate the load, which was then evenly distributed between the nodes along the top of the model. The load was held constant for all nine runs.

III. EXPERIMENTAL PROCEDURE

General Remarks

Rock cores were prepared for no-load crack density determinations and for uniaxial compression testing. Some of the cores which were prepared for compression testing were loaded to their ultimate strength while others were stressed to certain percentages of the ultimate strength. The latter specimens were tested using two end-platen configurations conforming to those used in the finite element models. The specimens that were stressed to a level less than the ultimate strength were quartered; one section was then prepared by hand-lapping for eventual examination of crack density. A point-count apparatus used at the Waterways Experiment Station (WES) for determining air-void content in hardened concrete was used for examining these sections. After a cursory examination of five sections, a criterion for identifying different types of cracks was developed. The criterion is comparable in part to that used by Willard and McWilliams (1969). Several schemes for presenting the crack density data were tried; these schemes plus the final one will be discussed later in this chapter.

The rock core used in this study was surplus from a WES rock mechanics program conducted in early 1969 (Saucier and Ainsworth, 1969). The core was NX size (2-1/8-in. diameter) and was diamond-drilled from one hole. The hole from which the core was taken is located in Albany County, Wyoming, township 14N, range 71W, section 23; the core was designated as CR-39. The rock was pre-Cambrian and very similar to the Sherman granite facies of the southern Laramie range.

Results of a petrographic examination showed the rock to be a coarse-grained granite. It is light-gray to pinkish-gray in color and

composed of quartz, potassium feldspar, plagioclase feldspar (probably

oligoclase), and biotite with minor amounts of hornblende and other

darker colored minerals. The rock is quite competent; however, on a

freshly sawed surface, numerous short, narrow cracks can be seen.

These cracks gave a relatively high crack density for the no-load speci-

mens, but this presented no problems during the study. Figure 4 shows a

photograph of a typical sawed surface of the test material.

Test Specimen Preparation

Twenty-six pieces of core were selected for this study. Ten speci-

mens were selected at random from the samples for determination of ulti-

mate compressive strength. The quantity of specimens chosen was based

on ASTM D 2938-71 (1971) preferred number and on the findings of Saucier

and Ainsworth (1969). These investigators reported that the compressive

strength of samples tested from hole CR-39 was "unusually consistent."

They reported an average C_o of 20,940 psi for nine tests. A standard

deviation of a single observation (s) and a range (R) were computed for

their data and were found to be 687 psi and 1860 psi, respectively. It

was concluded, therefore, that ten specimens of a rock with such low

values of s and R would be adequate to describe the ultimate com-

pressive strength. The remaining 16 specimens were used for the no-load

crack density determination and for compression testing.

Average values of the mechanical properties C_o , T , E , and

ν , which were used as code input data, are presented in Table 2;

statistical data showing dispersion are also included. The average

$(\bar{x})$ experimental data were reported by Saucier and Ainsworth (1969);

the statistical parameters (s) and (R) were calculated by this author.

Saucier and Ainsworth's (1969) direct tension and the C_o tests were
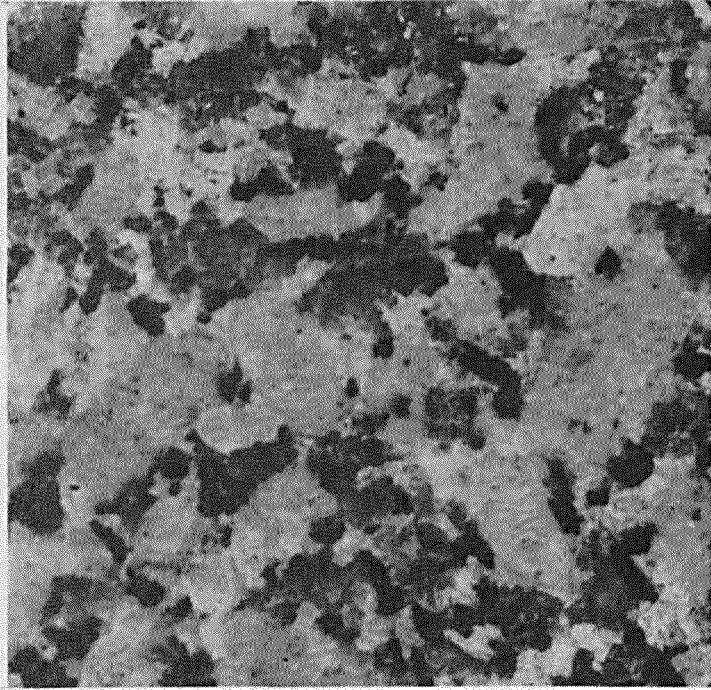
Magnification 1X

Figure 4. Photograph of a Sawed Surface of Core Showing No-Load
Crack Distribution

TABLE 2

Average Mechanical Property Data

Physical Property	Number of Specimens	Statistical Values		
		$\bar{x}$	s	R
C_o	9	20,940 psi	687 psi	1860 psi
T	3	815 psi	36 psi	50 psi
E	3	8.65×10^6 psi	0.14×10^6 psi	0.34×10^6 psi
ν	3	0.26	0.01	0.03

conducted in accordance with ASTM D 2936-71 and D 2938-71 (1971),
respectively. Young's modulus and ν were calculated using the strain
readings obtained from two longitudinal and two transverse electrical
resistance strain gages (BLH, A-3-S6) which were bonded to the specimens
tested in compression. The gages were mounted 90 degrees apart around
the circumference and at the mid-height of the specimen. Specimen
stress was monitored using a linear potentiometer in association with a
Wheatstone bridge circuit connected by a mechanical linkage to the
weighing system of the 440,000-lb Baldwin universal testing machine
used. A double X-Y recorder was used to record stress and strain. The
longitudinal and transverse strains were averaged. Young's modulus was
calculated as a tangent value at $\frac{1}{2} C_0$ and ν was computed at the
same stress level.

In the present studies, all the specimens were prepared with an
L/D of 2. The specimens were cut to approximate length using a rock
saw having a diamond-impregnated blade; water was utilized as a coolant.
The ends were then ground flat to 0.001 in., parallel to each other and
at right angles to the longitudinal axis. Grinding of the ends was done
using a machinist surface grinder. A dial comparator was used to deter-
mine the planeness and parallelism of the ends and the perpendicularity
of the sides to the ends; test method CRD-C 62-69 in the Handbook for
Concrete and Cement (1949) was used for this purpose. The specimens
were allowed to air-dry for one week in the laboratory prior to testing
(air temperature was maintained at 73 $\pm$ 2 degrees, while the relative
humidity was maintained at 65 $\pm$ 5 percent).

Test Procedure

Presented in Figure 5 are the laboratory test configurations which
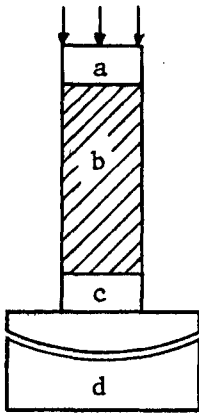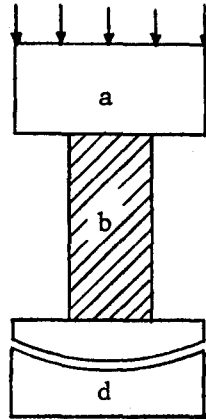
(a) Case 1, $D_p/D_s = 1$ (b) Case 3, $D_p/D_s = 3$

a Top Platen
b Specimen
c Bottom Platen
d Swivel Base

Figure 5. Laboratory Test Configurations for Problem 1 (L/D = 2).

were used for compression testing; these tests duplicate in size the appropriate finite element models. Only two test setups are presented in Figure 5; e.g., Problem 1 with Cases 1 and 3. It was first thought that all nine of the finite element models would be reproduced and tested in the laboratory; however, due to the limited time available and because Problem 1 (L/D = 2) is the most widely used L/D ratio for rock testing in the United States, only Problem 1 was run. The reason only Cases 1 and 3 were reproduced for testing is because of the results obtained from the finite element models. These results will be discussed in detail in Part IV. Briefly though, the load level at which yielding initiated in Cases 1 and 2 was identical, while in Case 3 yielding occurred 5 percent earlier than it did for Cases 1 and 2. Therefore, it was felt only necessary to run Cases 1 and 3.

In all tests, a swivel base* was used to insure concentric loading of the specimen. The end platens used in the compression test are illustrated in Figure 5. In Case 1, two plates were fabricated from bar stock of carbon steel (AISI Type C 1015) to have dimensions of 2 in. thick by 2-1/8 in. in diameter. The steel had a yield point of 46 ksi and a Rockwell hardness of 60 plus. For Case 3, a piece of 6-in. bar stock with the above-mentioned properties was used to fabricate a 2-in.-thick top end plate and the 6-in.-diameter swivel base itself served as the bottom end plate.

A Baldwin universal testing machine with a rated capacity of 440,000 lb was used to apply a compressive stress to the specimens. The stress was applied at a constant rate of 50 psi/sec. Ten specimens were tested for C_o using a $D_p/D_s = 1$. The average C_o was found to be

---

* Soiltest, Inc., Evanston, Illinois.

20,990 psi and the s and R values 1020 psi and 2800 psi, respec-
tively. These results are in good agreement with the data reported
earlier by Saucier and Ainsworth (1969) which further substantiates the
consistency of the rock.

An analysis of the theoretical model data showed that yielding
should be initiated at 78 and 73 percent of C_O for Problem 1, Cases 1
and 3, respectively. Considering these percentages and the information
presented in the Introduction, it was decided that for the Case 1 speci-
mens 80 percent of C_O would be the first applied stress level. From
this level on, the percentage of C_O would be increased 5 percent for
additional specimens. In other words, one of the five specimens would
be stressed to 80, one to 85, one to 90, one to 95, and one to 100 per-
cent of C_O . The stress was applied at a rate of 50 psi/sec to the
rated stress and then released at the same rate. Case 3 specimens were
stressed similarly with the exception that six specimens were tested,
and the starting stress level was 75 percent of C_O . No premature
failures occurred.

Specimen Preparation After Testing

The five no-load and the eleven stressed specimens were individu-
ally sawed into quarters. A cut was made at the mid-height normal to
the longitudinal axis, then parallel to the longitudinal axis. The
specimens were appropriately marked so that the center and top could be
referenced at a later time (see Figure 6). The surface examined for
cracking coincided with the surface examined in the finite element
models. It was believed that, if failure developed either as a double
cone or as tensile splitting, it could be easily traced. Another alter-
native was to cut the specimen into disks and examine each disk; however,

Direction of
Applied Stress

Longitudinal Axis

Top

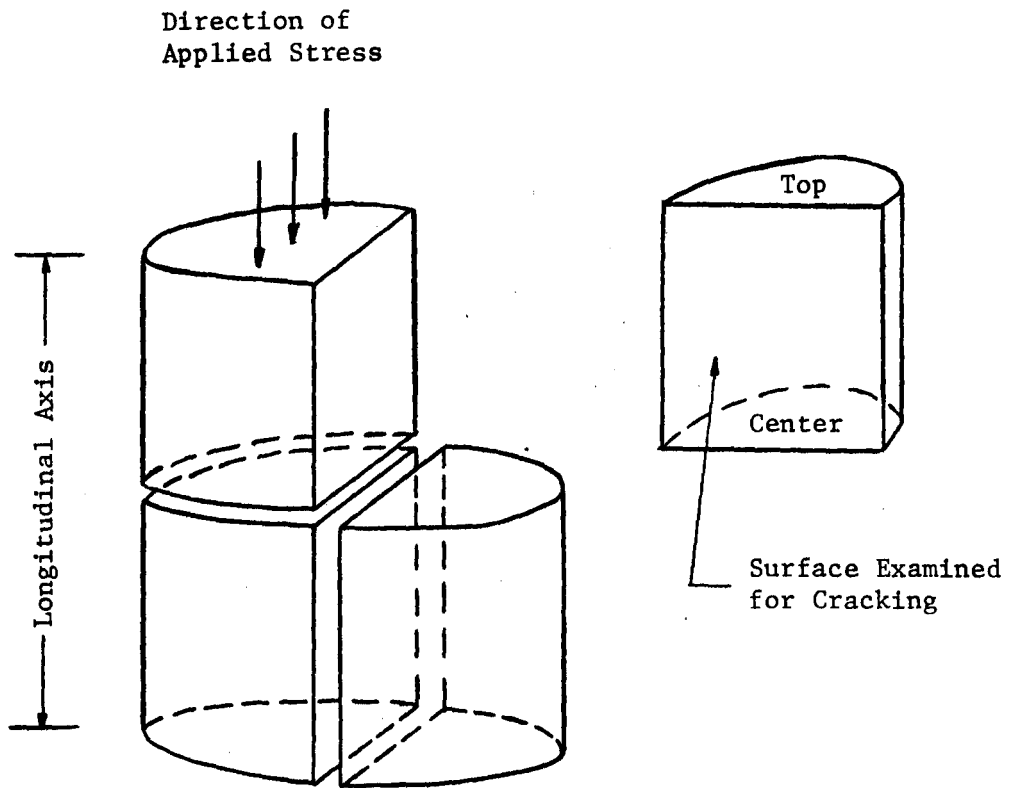Center

Surface Examined
for Cracking

Figure 6. Quartering of No-Load and Stressed Specimens
Prior to Microscopic Examination.

this would have been more time consuming and possibly not as suitable as the method used.

One-quarter section of each specimen was hand-lapped using a series of plate glasses and four different Carborundum grit sizes; numbers 220, 320, 450, and 600 were used. The coarser grits were used to remove all traces of the saw cuts, while the finer grits were used to obtain highly polished surfaces.

Air-Void Content Apparatus

A technique used in the Concrete Laboratory at the WES for determining the air-void content of hardened concrete was utilized to examine the polished surfaces for cracks. The technique is covered in detail in the Handbook for Concrete and Cement (1949) test method CRD-C 42-71. The main feature of the apparatus is the motorized mechanism which allows a flat carriage to be moved at 1/8-in. increments in two different directions. The apparatus has an independent stand from which a binocular microscope with 40X objectives can be extended to any fixed point over the carriage. Thus, the microscope remains fixed while the carriage is moved by 1/8-in. increments in the X or the Y plane. The field of view at 40X is just over 1/8 in. square. By placing a quartered section of core beneath the microscope and superimposing a 1/8-in.-square grid, the entire surface could be viewed without any overlapping. The grid was provided by placing a 3/32-in.-thick piece of window glass on the specimen. The window glass was 2-1/8 in. square and had a 1/8-in.-square grid scribed on one side; scribing was done using a diamond-tipped stylet. The total number of squares was 289. Figure 7 illustrates grid dimensions and grid numbers. The apparatus with a specimen and glass plate is illustrated in Figure 8.
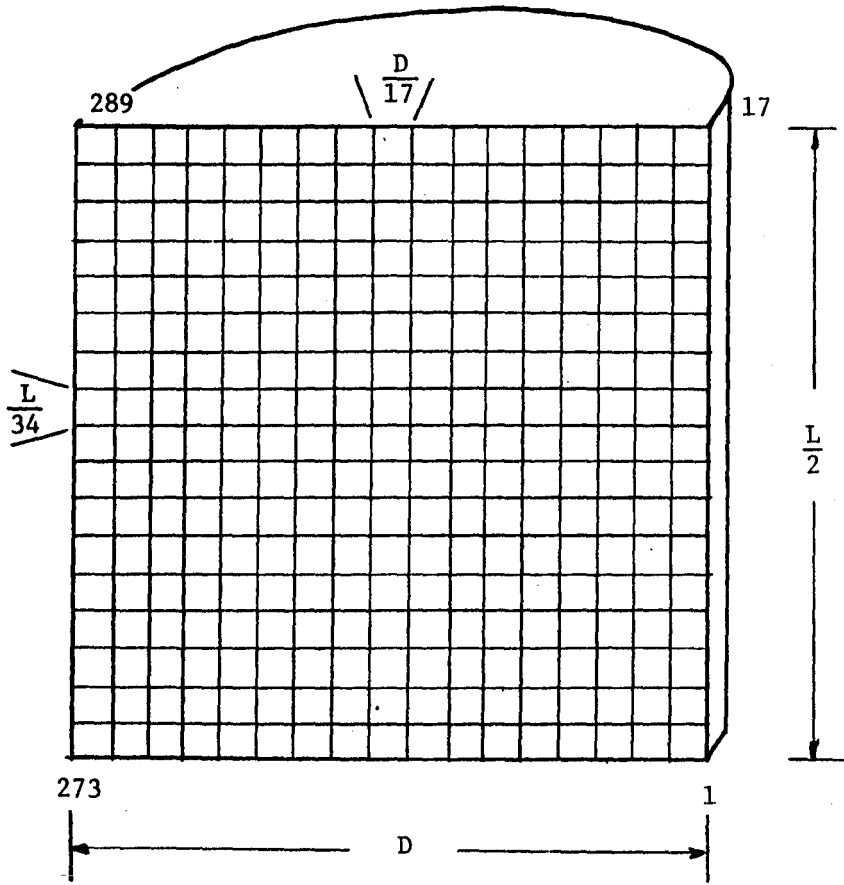
Top of Specimen

Figure 7. Section of Core Showing Sawed Surface, Grid
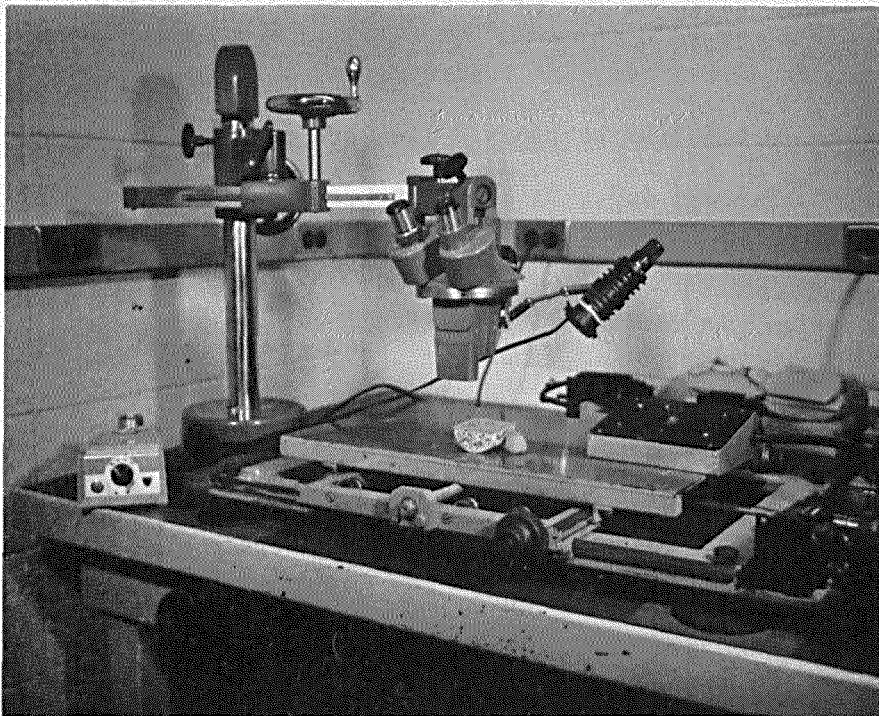   Dimensions, and Grid Numbers.

Figure 8. Air-Void Content Apparatus with Specimen.

Criteria for Crack Density

A cursory examination of the five no-load sections was made to determine what features should be included in a crack density scheme. The examination revealed that fractures and defects in the rock fabric were common to all five sections. The word crack is a descriptive term including fractures; e.g., "a break or breaking; as a chink or fissure; a narrow breach; a crevice; as in glass." The word crack also describes a defect; e.g., an inclusion plane in a feldspar crystal can be visible as a narrow breach, thus causing imperfection in the crystal. Now, if we describe the types of fractures and defects observed in this poly-crystalline rock, we can henceforth collectively refer to them as cracks.

Conchoidal fractures in quartz were not common. Some conchoidal fractures did, however, occur when quartz grains were located at the outer edges of the sections. It is assumed that these fractures were mainly caused by the sawing and preparation procedures. The most common fractures were those where total cohesion was lost, causing either rupture of a mineral or a break through a number of minerals. These fractures were evident as transgranular (passing through grains) or intergranular (following grain boundaries) fractures, and were observed as planar and irregular features. Defects in the rock fabric appear as planar and linear discontinuities associated with certain minerals. The defects identified and used by Willard and McWilliams (1969) were similar to those identified and used in this study. The defects are given below with the respective minerals. Mica and dark-colored minerals are collectively termed dark minerals (DM).

1. Quartz:

   a. Microfractures.

   b. Inclusion planes.

   c. Grain boundaries.

2. Feldspar:

   a. Cleavage planes.

   b. Inclusion planes.

   c. Grain boundaries.

3. Dark minerals:

   a. Flakes or traces of flakes.

   b. Cleavage.

   c. Grain boundaries.

Procedure for Recording Cracks

Sixteen sections (5 no-load and 11 stressed) were examined for total number of cracks detectable at 40X magnification. Cracks occurring in quartz, feldspar, DM, and occurring as intergranular features were recorded separately for each of 272 1/8-in. squares. The glass plate had 289 (17 rows and 17 columns) squares. The reason only 272 squares were used is because of the crushing which occurred in the top 1/16 in. of each specimen. The crushing is the result of the sawing technique used and not due to the stressing of the specimens.

The glass plate was taped to the section and the section positioned under the microscope. The piece of core was placed on four pieces of modeling clay and moved about until the section was level. It was then rotated in the X-Y plane until square No. 1 was within the field of the microscope and columns and rows could be traversed without misalignment. After examination of the first row, the carriage was returned, moved up

one column, etc., until the entire section was viewed.

During the examination of the polished sections, a great majority of the observed large fractures were oriented parallel to the longitudinal axis. In a few instances, fractures near the top and outside edge of the specimen were oriented toward the corners of the specimen. These fractures were generally macroscopic. Figure 9 illustrates typical types of cracks observed during this study.
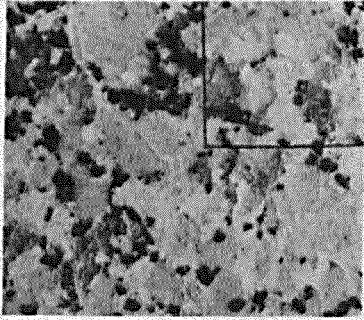
1X of Specimen 1-5 Stressed to 100 Percent C_o

2.5X of Specimen 1-5 Stressed to 100 Percent C_o

FELDSPAR

INTERGRANULAR FRACTURE

TRANSGRANULAR FRACTURE

QUARTZ
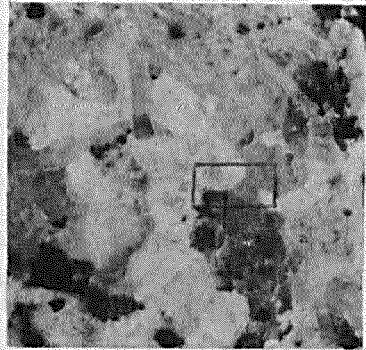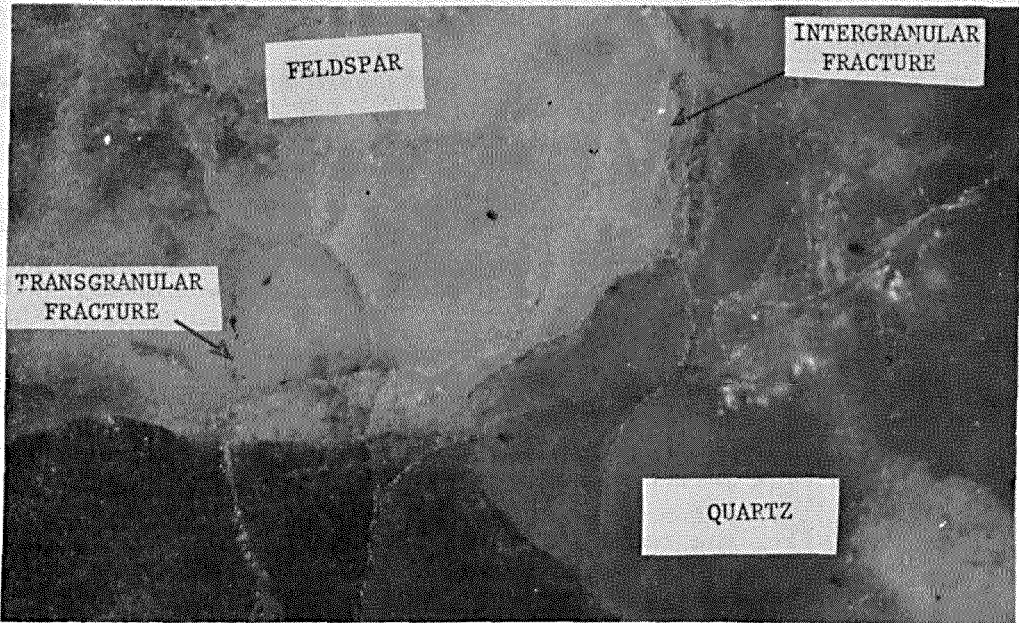
40X of Specimen 1-5 Stressed to 100 Percent C_o

Figure 9. Photographs Showing Typical Types of Cracks Observed.

IV. ANALYSIS AND DISCUSSION

The main purpose of this study was to determine the initiation and the propagation of failure in a circular cylinder of rock subjected to uniaxial compression. Theoretical and laboratory models were utilized in accomplishing this purpose. Nine theoretical models were analyzed for the influence of specimen L/D and D_p/D_s ratios upon: (1) stress trajectories, (2) the initiation of failure, and (3) the propagation and the extent of failure. Two of these nine models were reproduced in the laboratory, tested, and were analyzed for the propagation and the extent of failure. The results of this study are presented in this chapter, and in particular, the results of the two laboratory models are compared with the appropriate theoretical models.

Finite Element Models

Earlier work by the author (Stowe, 1969) has shown several interesting aspects concerning the construction and running of finite element models similar to the ones analyzed herein. In the previous work, a rock specimen $(L/D = 2)$ was modeled using end platens with various insert materials. The materials were constrained within a shallow cup-like platen and consisted of teflon, brass, aluminum, steel, and rock. The rock insert material was identical to the modeled rock specimen. Briefly, the results indicated that:

1. The teflon inserts caused very high compressive axial and tensile radial stresses to occur on and adjacent to the longitudinal model axis.

2. The brass, aluminum, and steel caused nonuniform loading across the top of the model.

3. The rock insert resulted in uniform stresses in the model.

In addition to these results, an important fact was realized. When a thin steel platen having a radius greater than the model radius was incorporated into the model, bending at the outermost edge of the platen occurred. This suggested that the platen was too thin or that, if displacement boundary conditions were used instead of force boundary conditions, the bending might not have occurred. However, in actual laboratory testing, bending of the platen does occur if too thin a platen is used. For this reason, the platen thickness used in the models reported in the present study was equal to two model radii. The platen was, therefore, overdesigned; however, very little bending of the platens was observed in the present study even when the $D_p/D_s = 3$.

Stress Trajectories

Stress trajectories (or isostatics) are lines parallel or normal to the two principal stress directions at all points through which they pass, and as such, they give a graphic representation of the directions of the principal stresses (Hetényi, 1950). The principal stresses, σ_1 and σ_3, are called the major and minor principal stresses, respectively. In this study, (−) denotes compression and (+) tension.

There was no appreciable effect of L/D ratio upon stress trajectories; however, there was a distinct effect of D_p/D_s upon trajectories when $D_p/D_s > 1$. Since constant ratios of D_p/D_s were used for all problems and since the trajectories in the platens are similar for all problems, Figures 10-12 are presented to adequately describe stress trajectories for all nine problems.

Figure 10 is a plot of the stress trajectories for Problem 2, Case 1 (L/D = 2.5, D_p/D_s = 1). The trajectories in the platen and in the specimen are vertical and horizontal except at the free boundary and
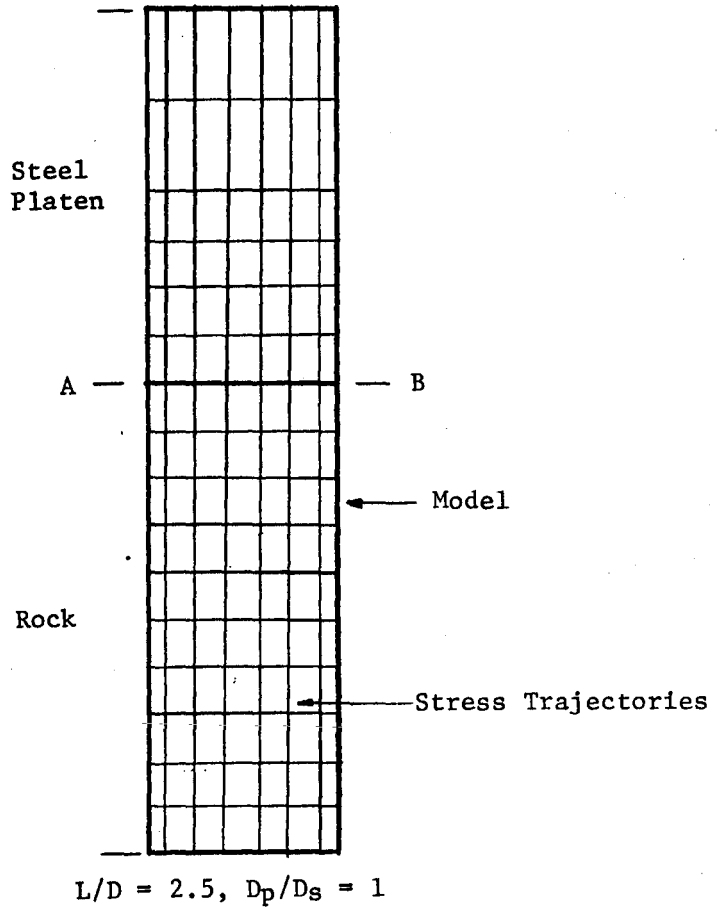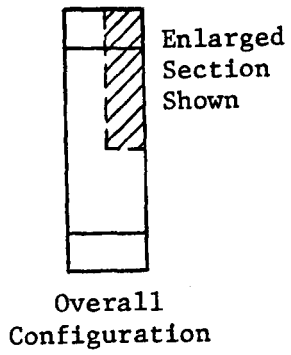
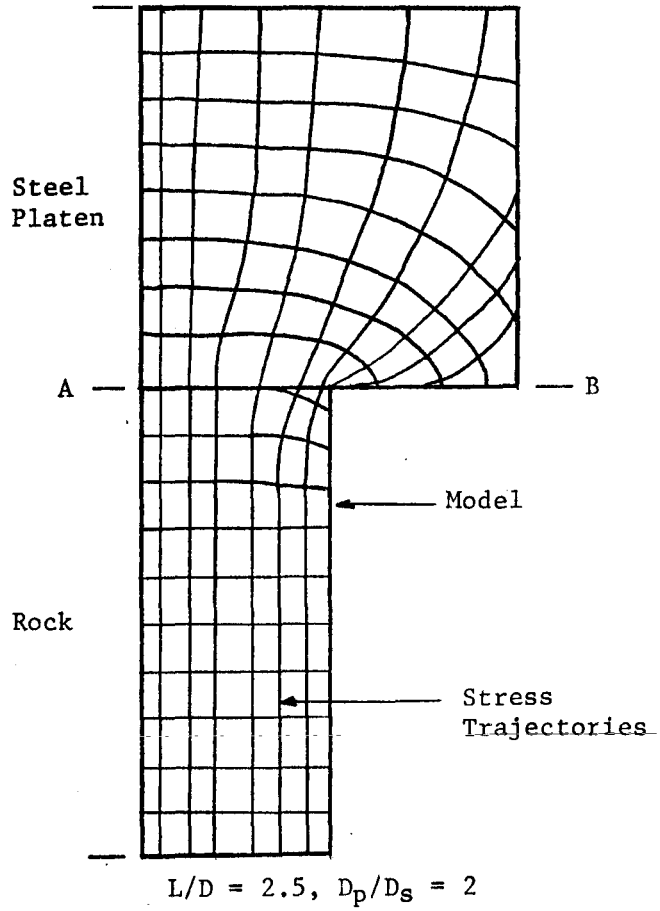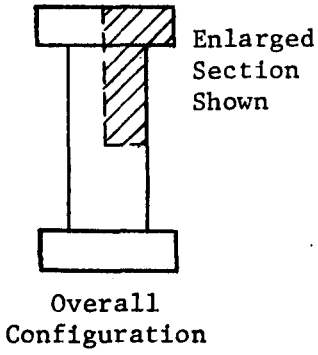Figure 10. Stress Trajectories for Problem 2 ($D_p/D_s = 1$).

Figure 11. Stress Trajectories for Problem 2 ($D_p/D_s = 2$).

Enlarged
Section
Shown

Overall
Configuration

Steel
Platen

A

B

Model

Rock

Stress Trajectories

$L/D = 2.5, \ D_p/D_s = 3$

Figure 12. Stress Trajectories for Problem 2 ($D_p/D_s = 3$).

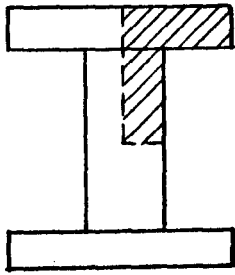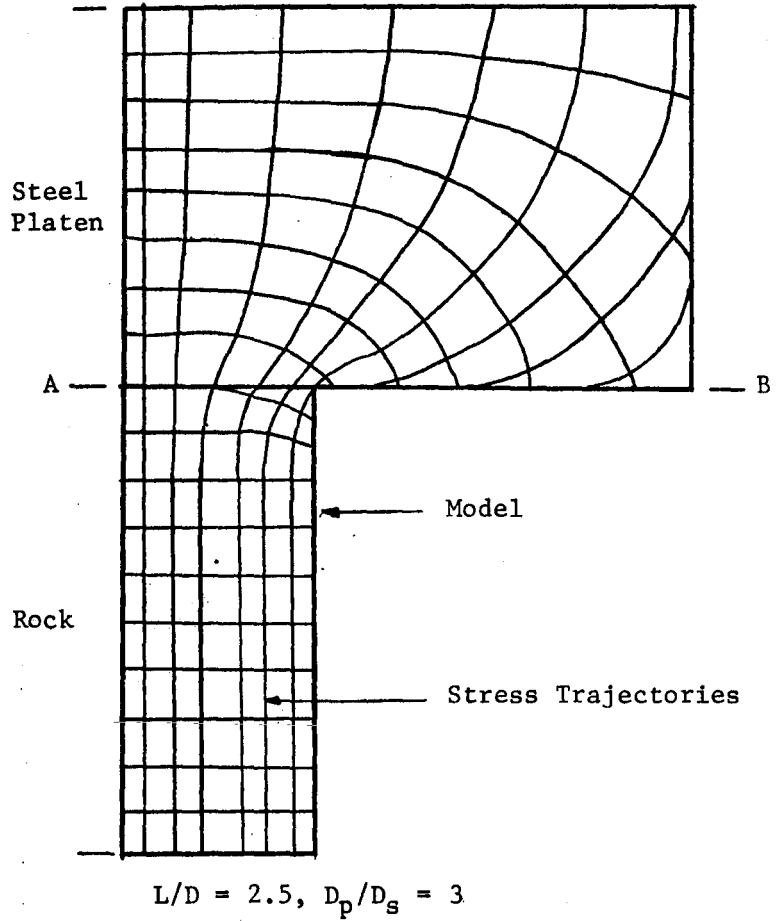near the platen-specimen interface. Here the direction of the major principal stress is less than 2 degrees off the vertical and the minor principal stress is off the horizontal by an identical amount. Radial end restraint, caused by the elastic mismatch between the steel platen and rock, accounts for the slight change in the direction of the principal stresses. The radial end restraint is due in part to Poisson's ratio; e.g., the strains in the rock in the radial direction are greater than in the radial direction of the steel platen. Therefore, the lateral expansion in the rock is resisted by the steel; hence, tensile stresses in the steel apply opposite compressive stresses to the rock.

Figures 11 and 12 clearly illustrate the effect of increasing the platen width greater than one specimen radii. The stress trajectories near the longitudinal axis of symmetry are vertical and horizontal. However, this is not the case in the platen and specimen as the free boundary is approached along the platen-specimen interface (A→B). The change in the direction of the principal stresses is greatest for the case where $D_p/D_s = 3$. The effect of D_p/D_s upon trajectories diminishes rapidly at 0.5 r in the specimen; the trajectories are nearly vertical and horizontal beyond 0.5 r (r is the radius of the test specimen).

Shear and confining stresses are highest in the areas where the trajectories deviate the greatest. Figure 13 illustrates a typical example. The four elements at the outer topmost corner of the specimen are shown. From the tabulation, it is clear that as D_p/D_s is increased to 3, shear and confining stresses increase, as do the other stress components. Elements below 0.5 r gradually become more uniform with respect to the values of these stresses. Shear and confining

37

Figure 13. Effect of D_p/D_s on Shear and Confining Stresses in Corner Elements for L/D = 2.
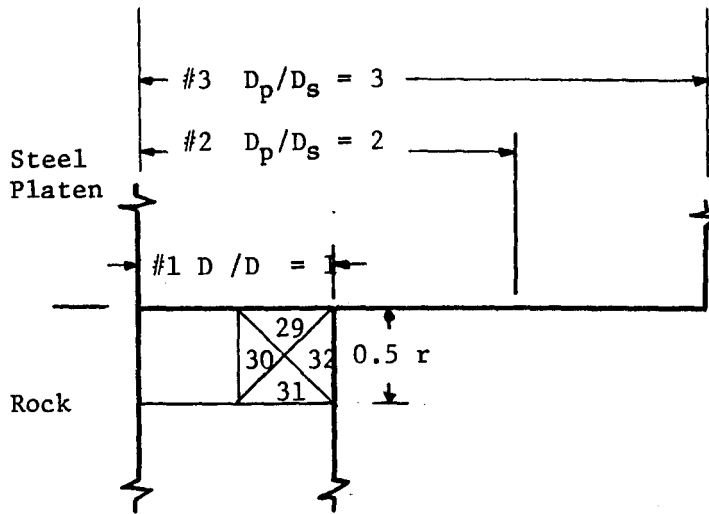
D_p/D_s	29	30	31	32
		Shear Stress		
1	969	625	917	1261
2	4223	2908	2885	4201
3	5972	4111	4083	5943
		Confining Stress		
1	−3576	−1992	−305	−1881
2	−6903	−4782	−959	−3252
3	−8924	−6283	−1170	−4247

38

stresses in elements between 0.5 r and 1.0 r decreased by almost an order of magnitude. The laboratory results show evidence of high confining stresses developing near the top of the specimen; the evidence is that there is very little cracking in this zone. This will be discussed later.

Initiation of Failure

The results of the finite element analysis indicate that the L/D and D_p/D_s ratios had no effect upon the location within the specimen at which failure initiated. Failure started in the center of all models. The stress level at which failure initiated, however, was found to be a function of L/D and D_p/D_s . Figure 14 illustrates the effect of these parameters upon this stress level.

For each of the L/D ratios used, the stress at which yielding occurred remained the same or increased where D_p/D_s = 2 , but decreased for D_p/D_s = 3 . For Problem 1 (L/D = 2) where D_p/D_s = 2 , the stress level remained the same; however, in Problems 2 and 3 (L/D = 2.5 and 3) , a slight increase in the stress at which first yielding occurred was observed. When the platen diameter was increased to three times the specimen diameter, the stress level at which yielding commenced decreased. The greatest decrease (5 percent) was observed for Problem 1.

It is believed that this low yield stress (73 percent of C_o in Problem 1) is due to the length of the specimen and radial end restraint. As an explanation of this statement, the following is offered. The greater the end restraint, the further a complex state of stress extends into the specimen (i.e., towards the center). With a short specimen length, these stresses cannot be readily dissipated, and
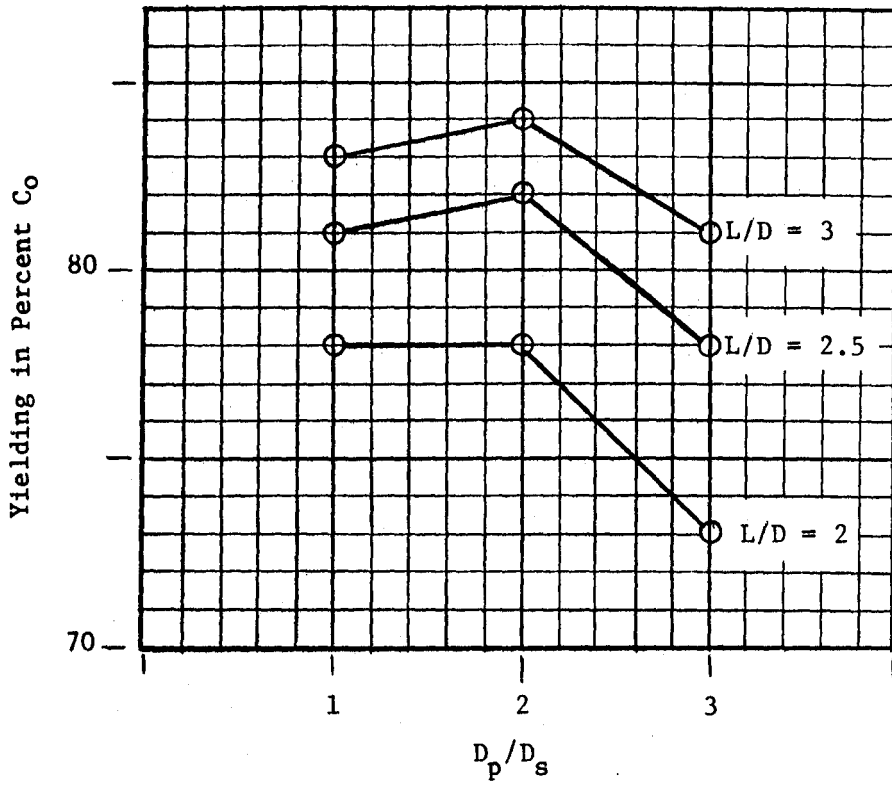
Figure 14. Yielding in Percent of C_O as a Function of D_p/D_s for Different L/D Ratios.

high stress concentrations could occur, causing early yielding. This suggests that a minimum L/D of 2 should be specified for compression testing. Hawkes and Mellor (1970) discuss results of many authors concerning L/D ratios for compression testing and conclude that an L/D = 2 is an absolute minimum. Results of this study, which are discussed in the next section, tend to verify these authors' conclusion.

Propagation and Extent of Failure

In all three problems, failure propagated upward and outward from its origin at the center of the model. Figures 15-17 show the typical progression of yielded elements for Problem 2 as D_p/D_s = 1, 2, and 3 . The symbols represent the different percentage of C_o at which elements yielded. A range of 4 percent was chosen for convenience.

Figure 18 summarizes for all the models the extent to which failure propagated; the effect of both L/D and D_p/D_s are clearly illustrated. Failure extended to within 1.0 r of the platen along the longitudinal axis of symmetry. This extension is independent of L/D and D_p/D_s with one exception. That exception is for L/D = 2 where D_p/D_s = 3 . It is believed that this exception is a result of the complex stress zone mentioned in the last section. In other words, the radial end restraint, resulting in high confining stresses, caused a repression of the failed zone. These high confining stresses do not cause the repression per se. Rather, the confining stresses account for an increase in the shear strength of the rock in this zone; hence, higher normal loads are required before failure could occur. However, before this happens, the failure zone has traversed those sections of the model where the shear strength is lower.
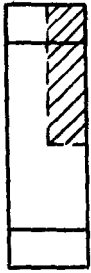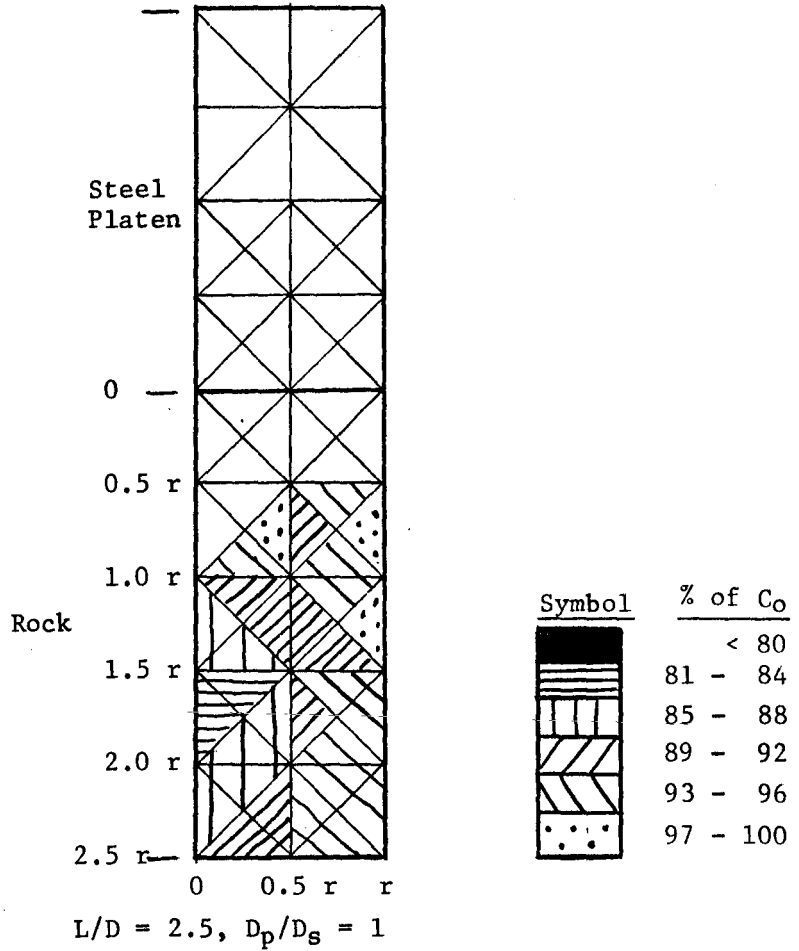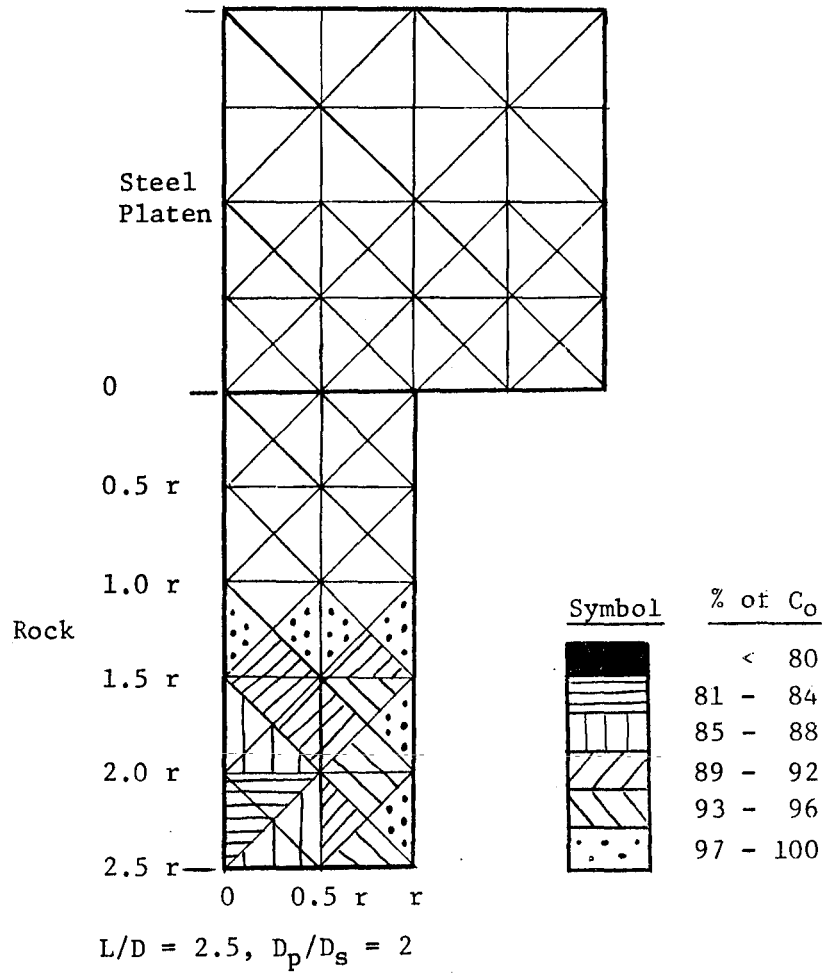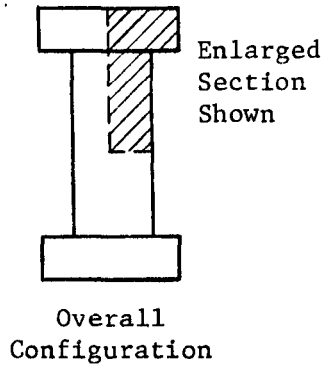
Figure 15. Progression of Yielded Elements for Problem 2 $(D_p/D_s = 1)$.

Figure 16. Progression of Yielded Elements for Problem 2
$(D_p/D_s = 2)$.

Enlarged
Section
Shown

Overall
Configuration

Steel
Platen

0

0.5 r

Rock

1.0 r

1.5 r

2.0 r

2.5 r

0   0.5 r   r

L/D = 2.5, D_p/D_s = 3

Symbol	% of C_0
	< 80
	81 – 84
	85 – 88
	89 – 92
	93 – 96
	97 – 100

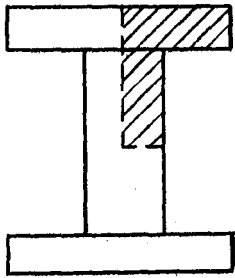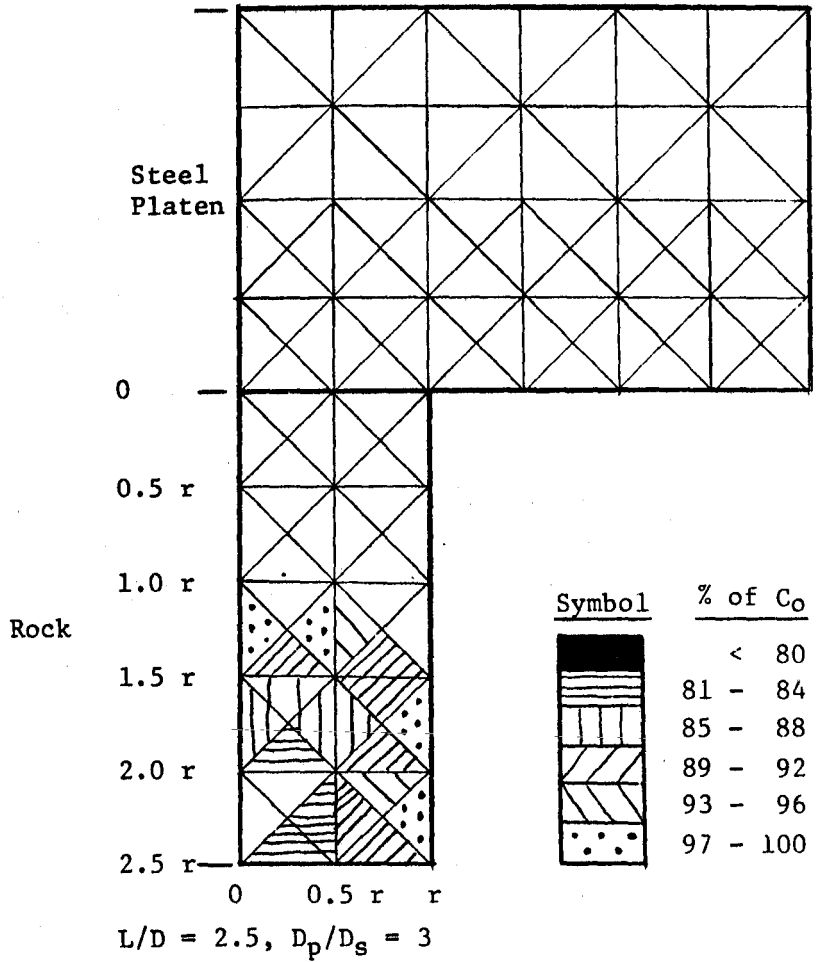Figure 17.   Progression of Yielded Elements for Problem 2
(D$_p$/D$_s$ = 3).

44

Enlarged
Section
Shown

Top of Specimens

0

0.5 r —

1.0 r —

1.5 r —

2.0 r —

2.5 r —

3.0 r —
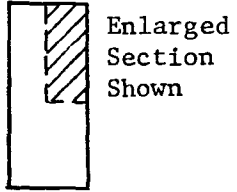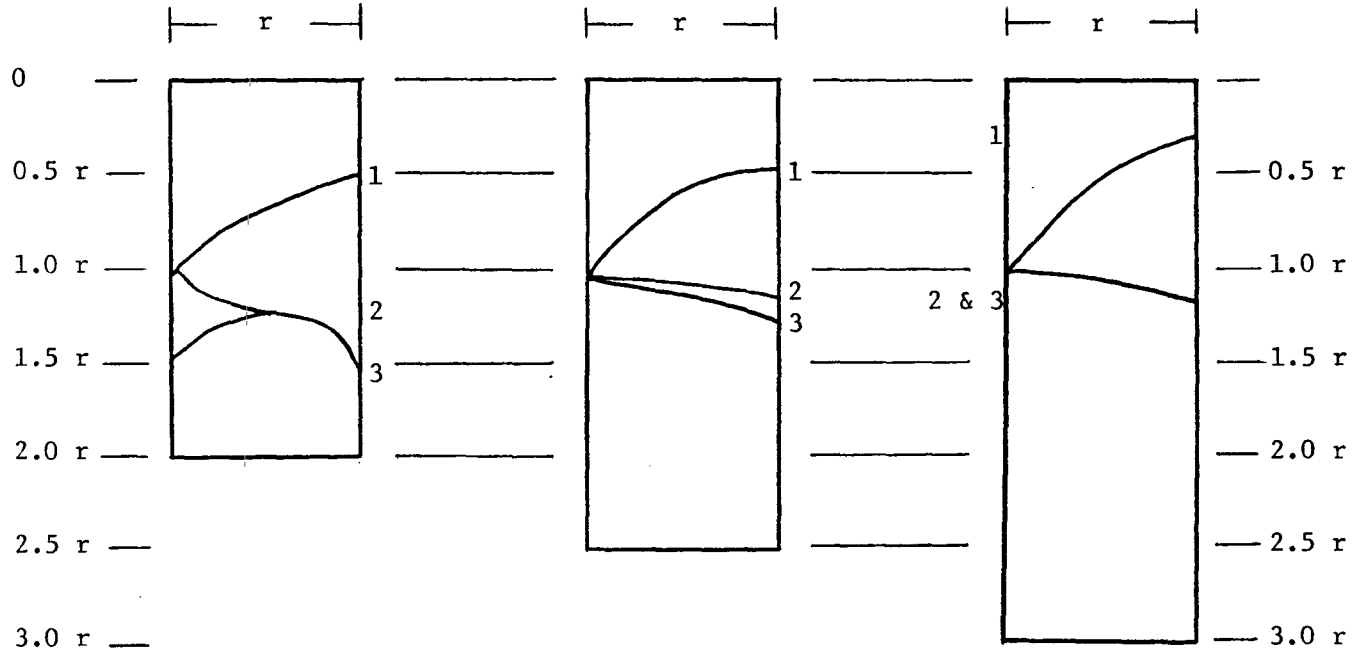
Problem 1
L/D = 2
D_p/D_s = 1, 2, & 3

Problem 2
L/D = 2.5
D_p/D_s = 1, 2, & 3

Problem 3
L/D = 3
D_p/D_s = 1, 2, & 3

Figure 18. Extent of Failure for All Models (r = Specimen Radius)

The extent of failure at the free boundary is dependent upon both L/D and platen width. A greater effect is seen for platen width. Failure propagated to within 0.5 r and 0.3 r of the platen for $D_p/D_s = 1$ in Problems 1 and 2 and Problem 3, respectively. The effect of a platen wider than the specimen is quite noticeable in all three problems. The points indicating the extent of failure at the free boundary for $D_p/D_s = 2$ and 3 are further evidence that a complex state of stress exists within the top one-third of the specimens. For Problem 1, this point is 1.5 r from the top of the specimen. From the results of the finite element models, it is evident that a $D_p/D_s = 1$ is superior for unconfined compression testing. In other words, a steel platen where $D_p/D_s = 1$ minimizes the effect of end restraint.

Laboratory Models

To reiterate, laboratory specimens with $L/D = 2$ and $D_p/D_s = 1$ and 3 were tested in compression, prepared by quartering and polishing, and examined for total number of·cracks. ·Originally, it was proposed to use one scheme for determining the crack density by 1/2-in. squares. However, the results obtained using 1/2-in. squares were inconclusive. Crack density was then calculated using 1/4-in. squares. This time general trends were indicated. It was believed that, by reducing the area further, the traces of failure might be detected. The crack density scheme (CDS) finally used was simply total cracking per 1/8-in. square. Both schemes will be discussed in the following section.

Crack Density Schemes

The first CDS incorporated the results of the no-load specimens. In this scheme, cracking in the stressed specimens was expressed as a percent of the average cracks observed in the unstressed specimens; i.e.:

$$\text{Crack Density} = \frac{A-B}{B} \times 100 \qquad\qquad (4)$$

where A is the total number of cracks at a percent C_o in a 1/2-in.

square and B is the average number of cracks at no-load in a 1/2-in.

square.   This scheme indicates an increase in cracking at a specific

location on the central plane of the stressed specimen. For any CDS to

be useful, an even distribution of the component parts of the whole

should exist, and this distribution should hold for each specimen. The

planes of the specimens which were examined appeared to have an even

distribution of minerals, and each specimen contained similar quantities

of quartz, feldspar, and DM (dark minerals).

After the crack densities were calculated for all stressed speci-

mens, a 1/2-in.-square grid similar to the one illustrated in Figure 7

was drawn up. Appropriate values were placed in their respective loca-

tions, and an attempt was made to contour points of equal value. At

this juncture, the following conclusions were made for the laboratory

models:

1. The amount of cracking in certain zones increased with

increased application of stress.

2. More cracking occurred in the central region of the specimens

than occurred near the top of the specimens. This is the first agree-

ment between the theoretical and the laboratory model.

3. A failure plane was not evident.

Crack densities were then recalculated on the basis of a 1/4-in.

grid. This was done for all specimens. The same procedure used above

was repeated in an attempt to contour the new densities. This attempt

resulted in some improvement. In addition to the above conclusions

(made using the 1/2-in. grid), the following were reached.

1. For both D_p/D_s ratios, the intensity of cracking in the central region of the specimens was quite discernible, especially so when the 75 and 80 percent stressed specimens were contrasted with appropriate specimens stressed to 100 percent C_o. The increase in cracking was not so apparent when comparing specimens stressed at 5-percent increments of C_o.

2. A noticeable decrease in cracking occurred for $D_p/D_s = 3$ at all five stress levels. The decrease occurred inside a diagonal line drawn from the top outside edge of the specimen to a point approximately 1.0 r from the platen on the longitudinal axis of symmetry. This point coincides with the one discussed earlier in the finite element model (see Figure 18, Problem 1, $D_p/D_s = 1$ and 2). This is the second indication that some agreement between the theoretical and laboratory models exist.

The above results were encouraging; however, it was believed that the areas being examined were still too large and that this was masking high and low density zones which could be indicative of a failure plane. It was, therefore, decided to re-examine the crack data on the basis of a 1/8-in. grid. This scheme simply entailed plotting the total number of cracks per 1/8-in. square and drawing contours. Crack density was then expressed as total cracks per unit area where the unit area for 1/8-in. grid is 0.0156 in.[2]

Propagation and Extent of Failure

Figures 19-23 and Figures 24-29 illustrate contours of crack density for $D_p/D_s = 1$ and 3 , respectively. Figures 19-23 represent the five specimens stressed at 5-percent increments of C_o starting
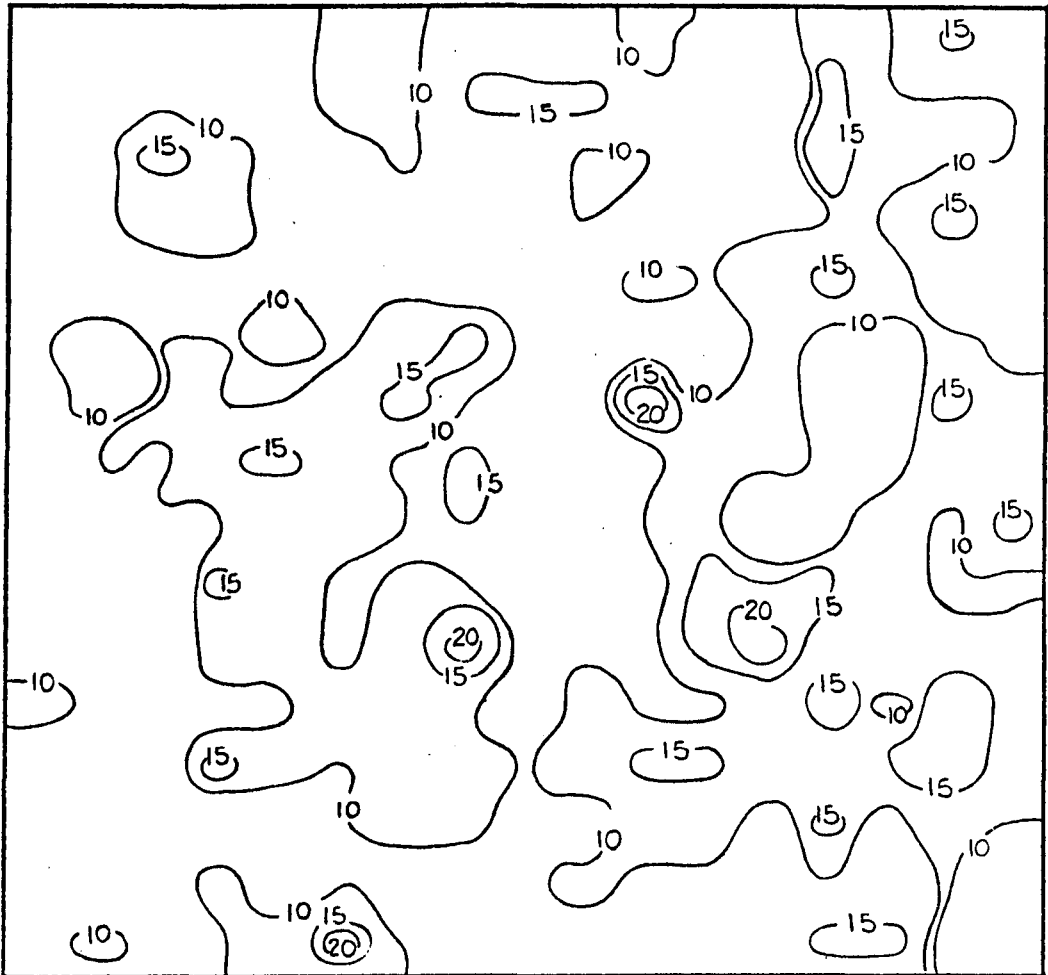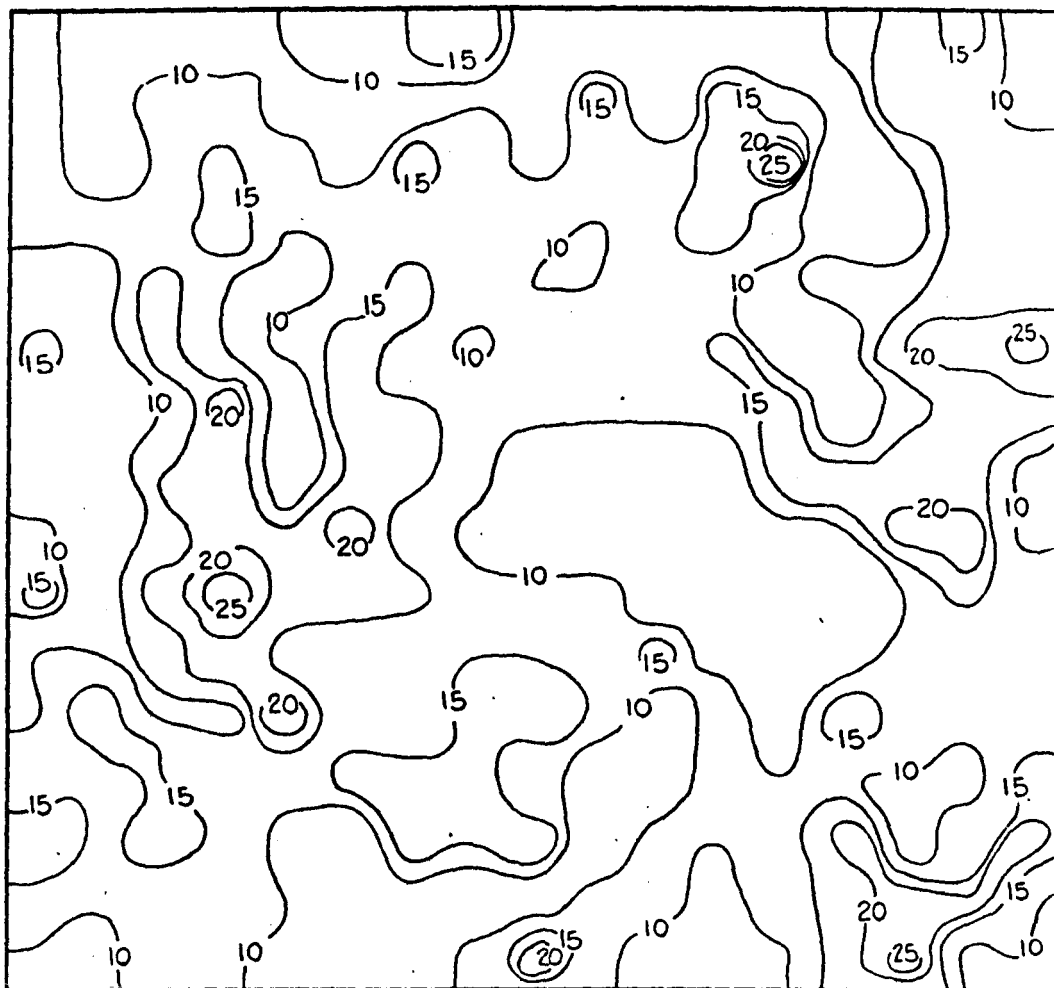
Stressed to 80% C_o

Figure 19. Contours of Crack Density, $D_p/D_s = 1$.

Stressed to 85% C_o

Figure 20. Contours of Crack Density, $D_p/D_s = 1$.

Stressed to 90% C_o

Figure 21. Contours of Crack Density, $D_p/D_s = 1$.

Top of Specimen

Stressed to 95% C_o

Figure 22. Contours of Crack Density, $D_p/D_s = 1$.

Top of Specimen

Stressed to 100% C_o

Figure 23. Contours of Crack Density, $D_p/D_s = 1$

Stressed to 75% C_o

Figure 24.   Contours of Crack Density, $D_p/D_s = 3$.

Stressed to 80% C_o

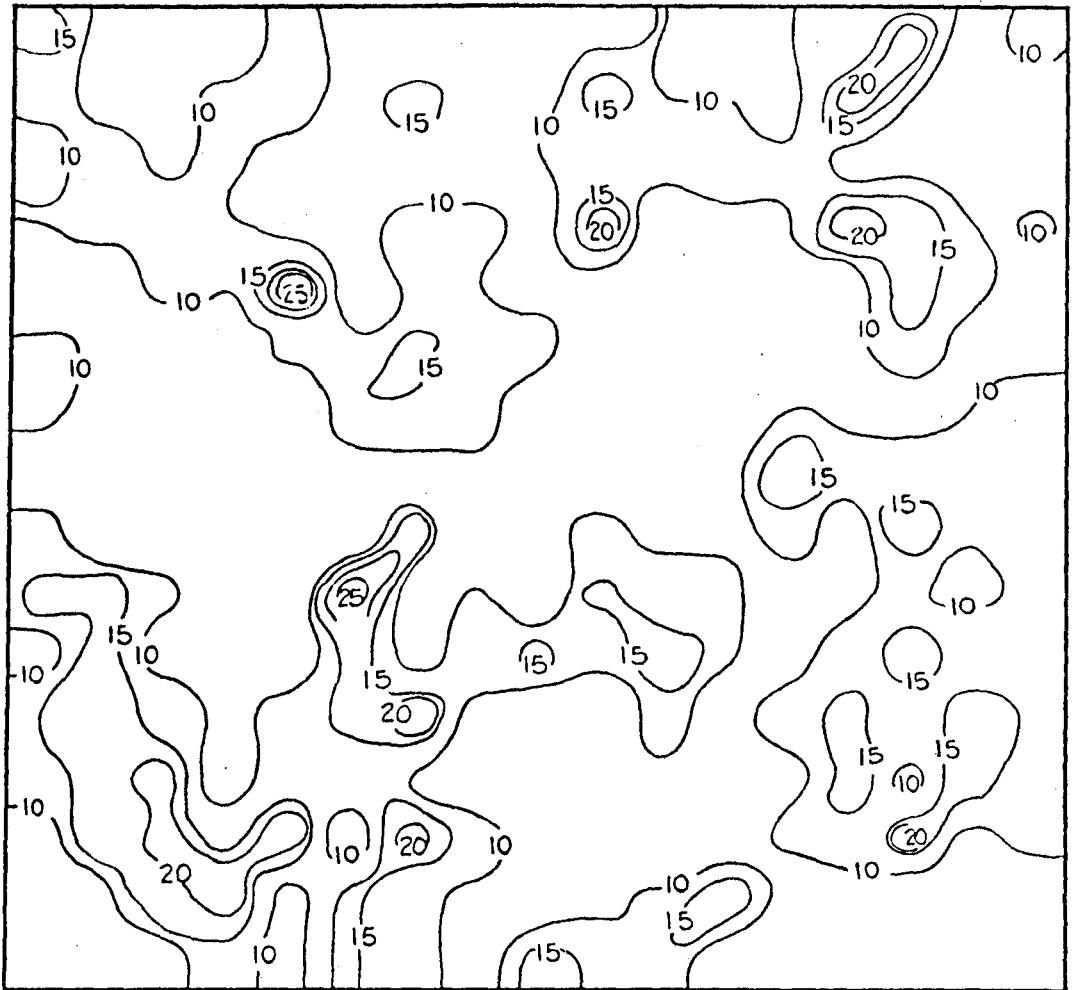Figure 25. Contours of Crack Density, $D_p/D_s = 3$.

Top of Specimen

Stressed to 85% C_o

Figure 26. Contours of Crack Density, $D_p/D_s = 3$.

Top of Specimen

Stressed to 90% C_o

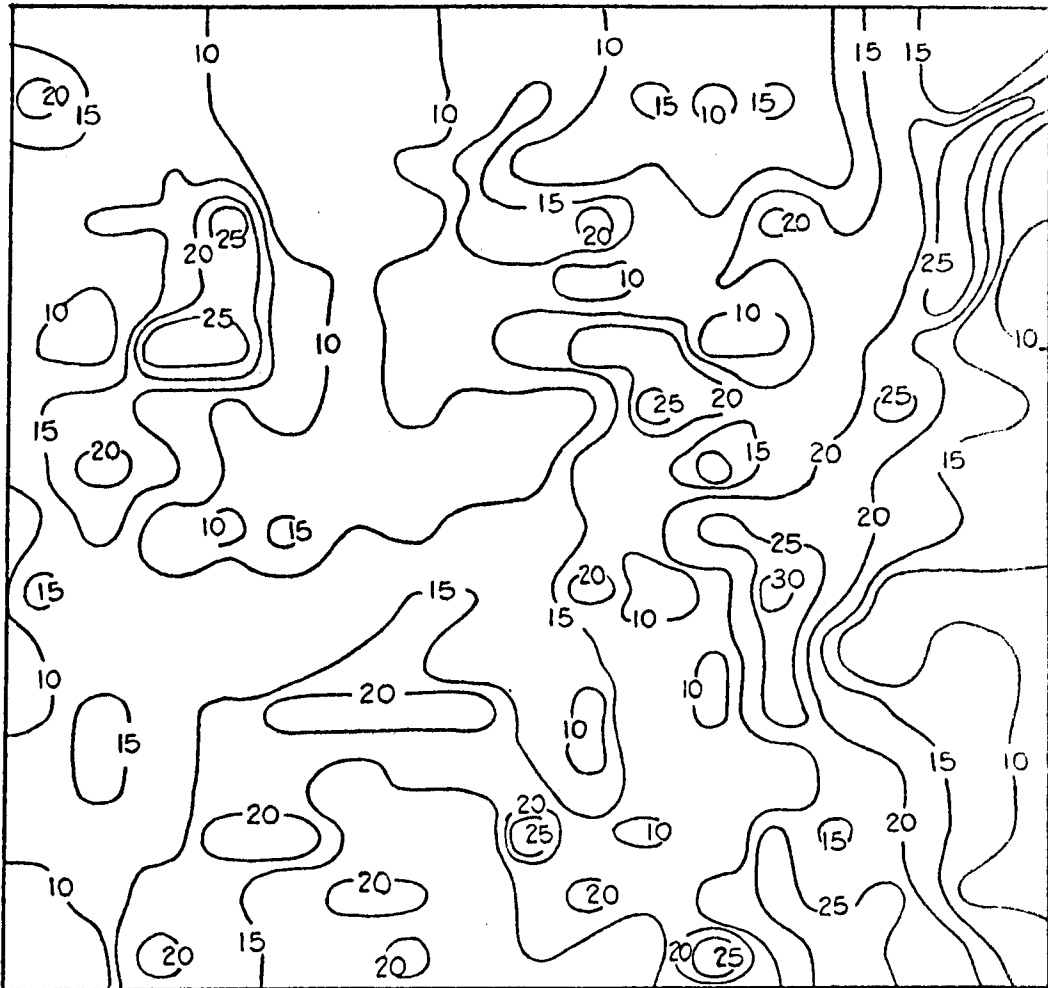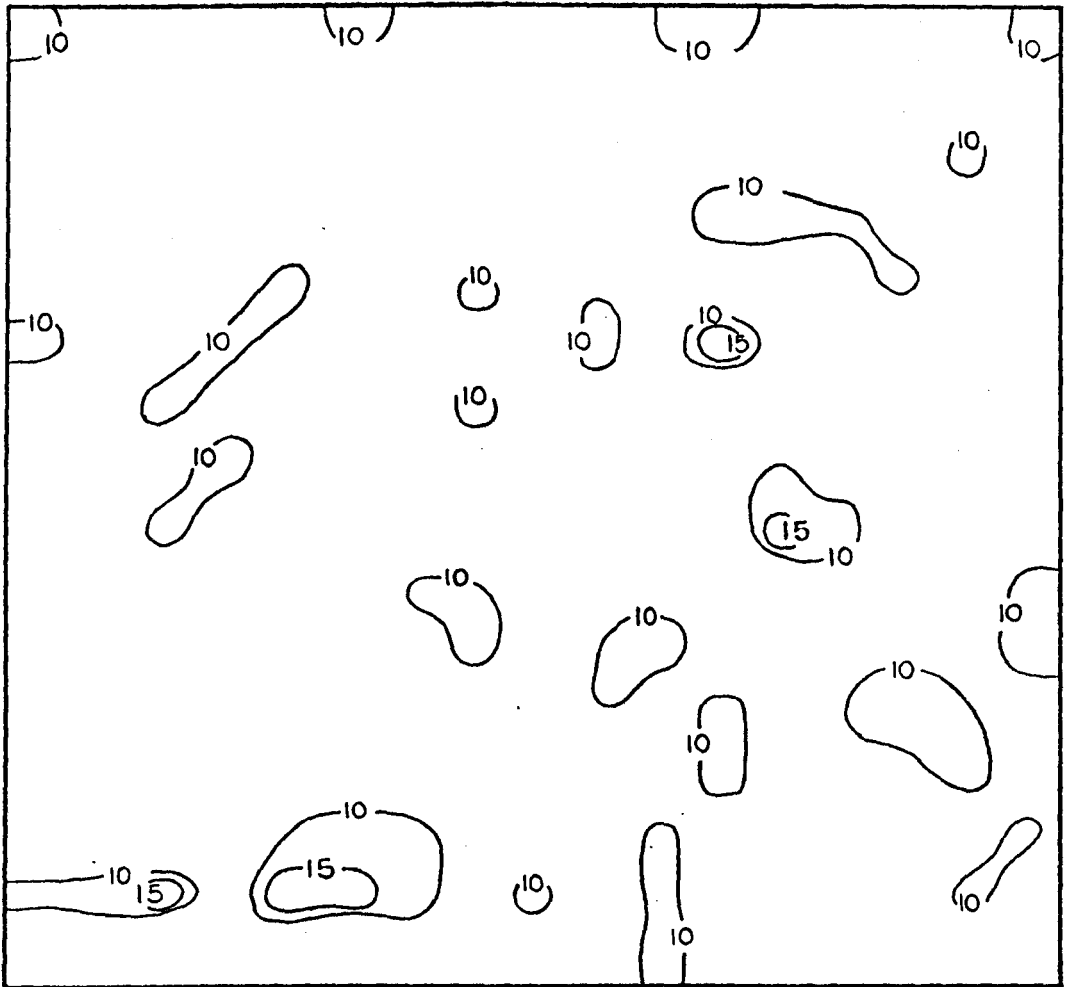Figure 27. Contours of Crack Density, $D_p/D_s = 3$.

Top of Specimen

Stressed to 95% C_o

Figure 28.   Contours of Crack Density, $D_p/D_s = 3$.

Top of Specimen

Stressed to 100% C_o

Figure 29. Contours of Crack Density, $D_p/D_s = 3$.
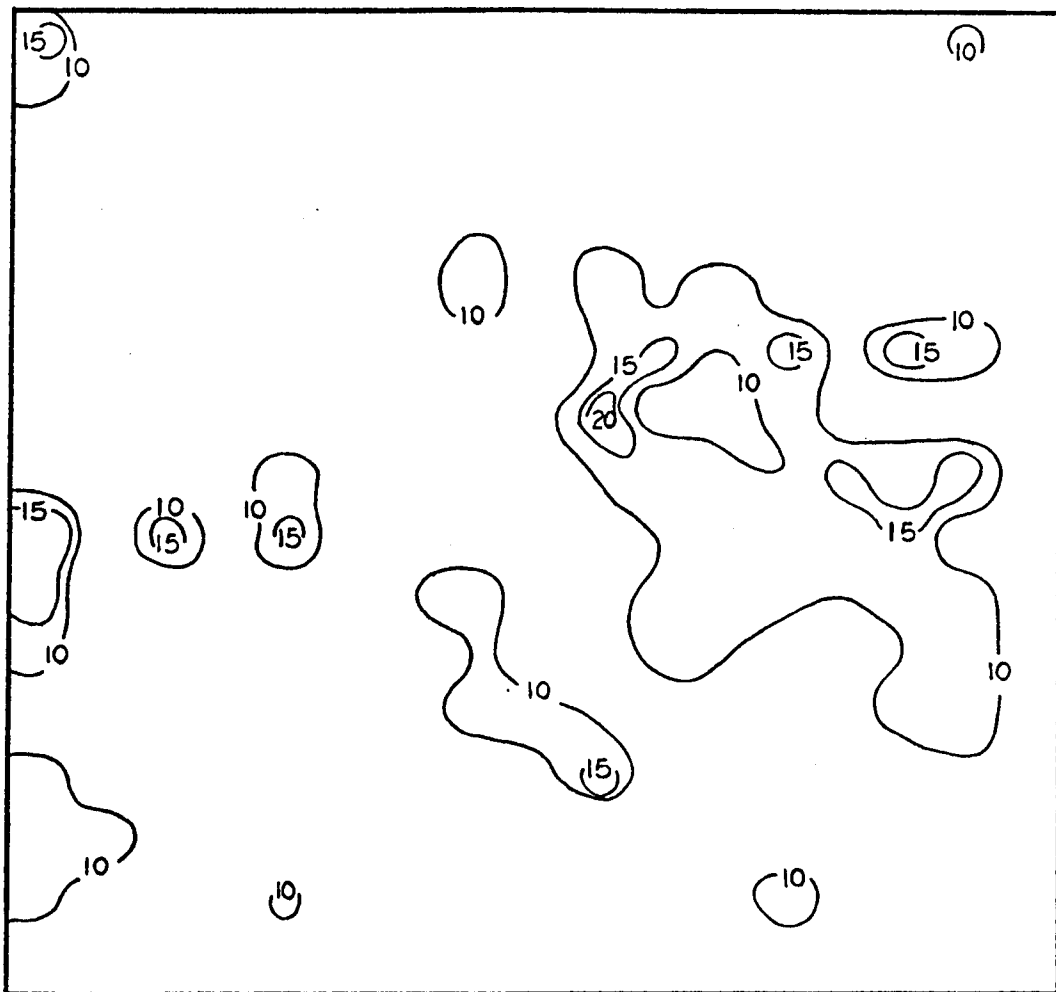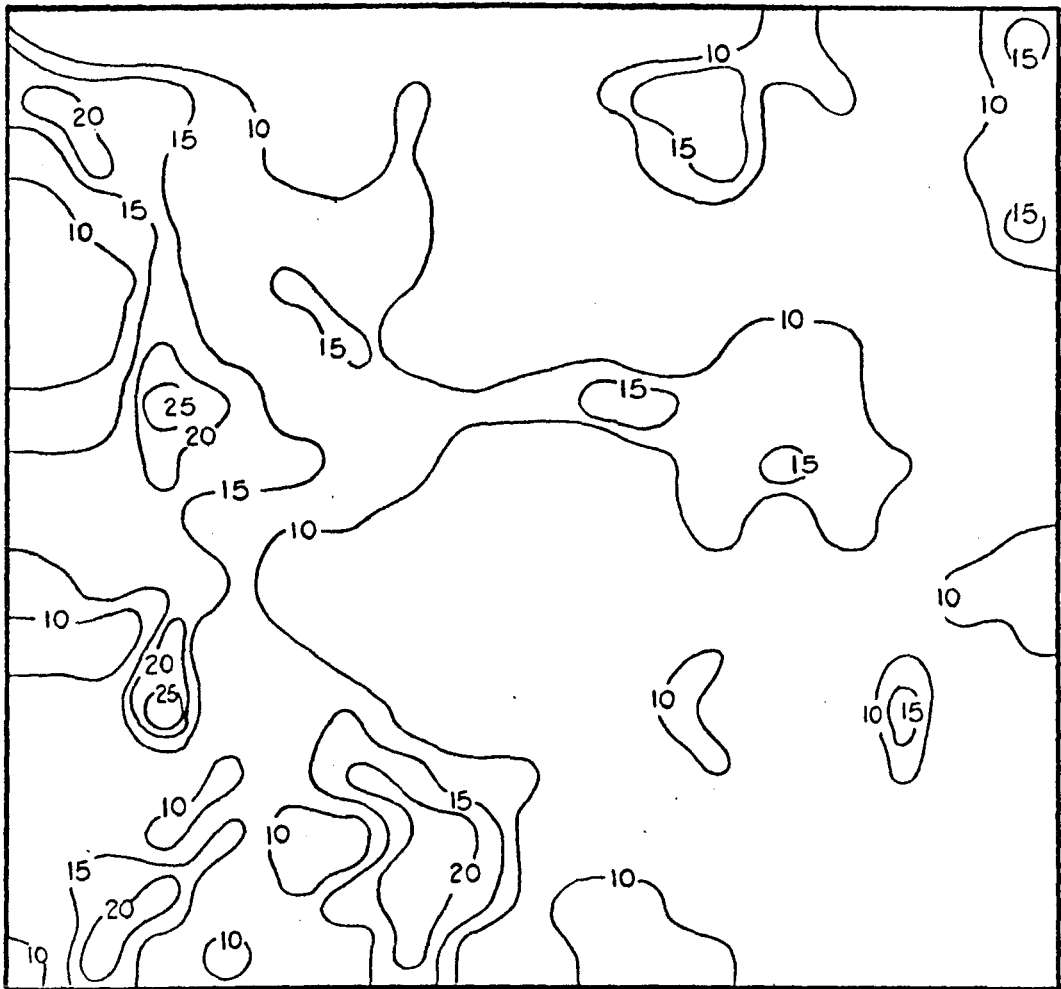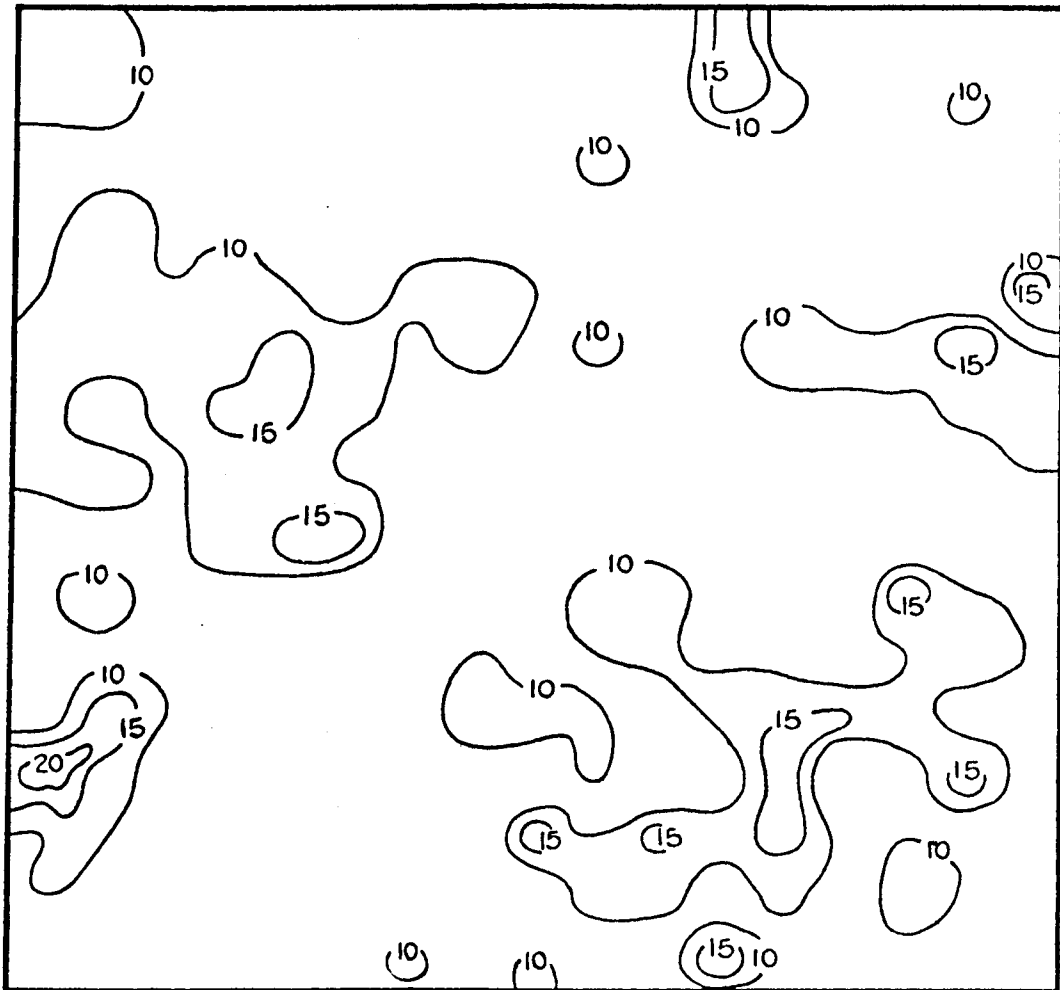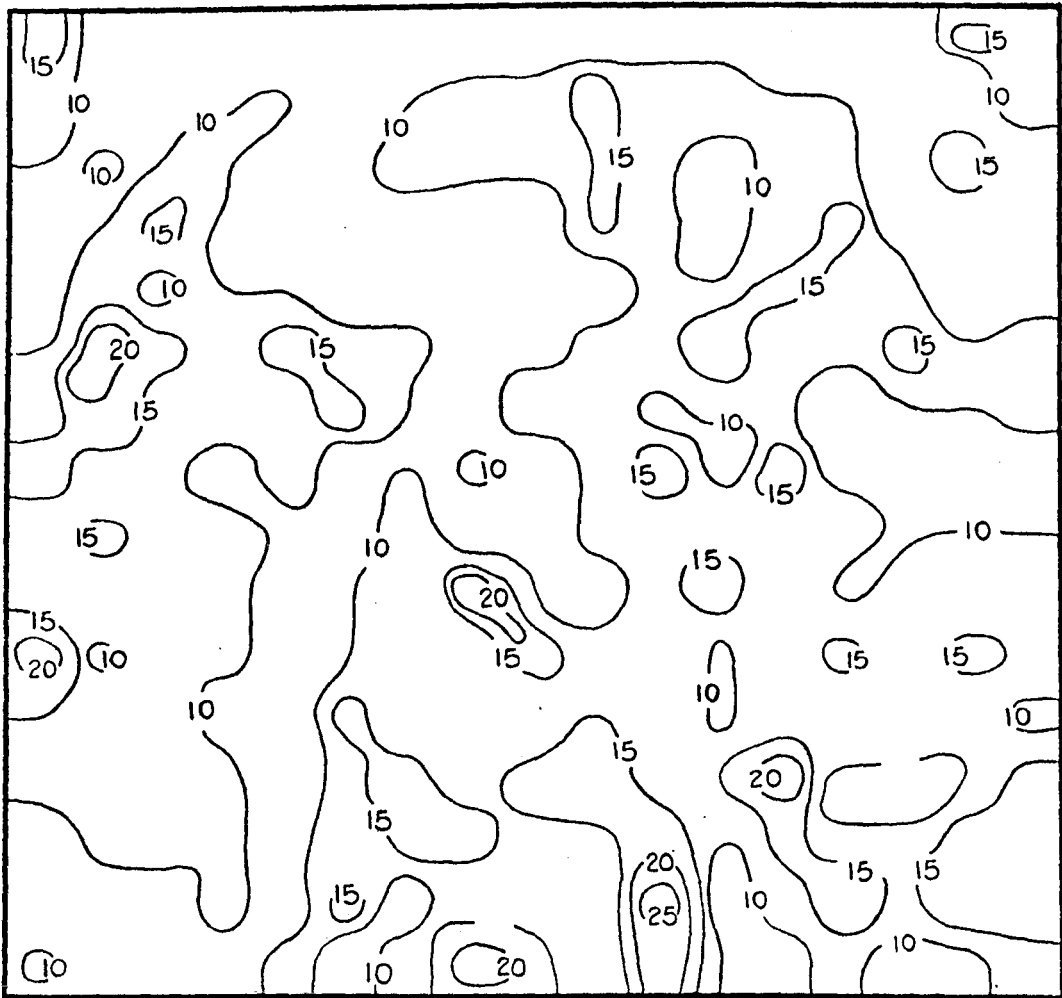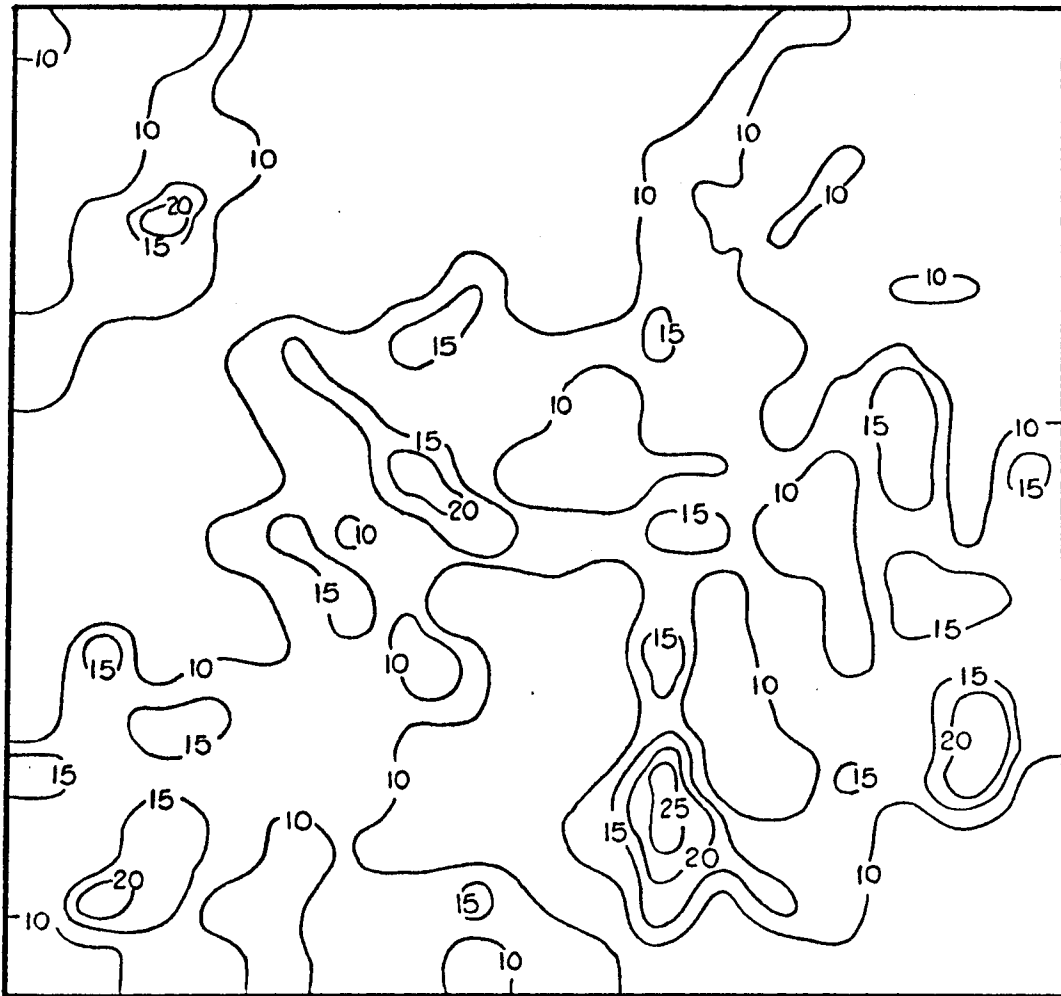
at 80 percent C_O . Figures 24-29 represent the six specimens also stressed at 5-percent increments of C_O but commencing at 75 percent C_O .

The no-load specimens showed that the average number of cracks per 1/8-in. grid equaled 8.4. Therefore, the contouring was begun with lines connecting points where crack densities equaled to ten; five density units were used for the contour interval.

The specimen stressed the least (see Figure 19) indicates that yielding has started in the central region and near the mid-height of the specimen. There are three 20-unit contour lines within this region. The remaining four specimens show an equal or greater number of such lines in the same region. In contrast to the least stressed specimen, the specimen stressed the greatest amount (see Figure 23) has nine 20-unit contour lines within this portion of the specimen. Three of these nine lines show 25-unit values.
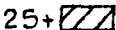
The progression of failure in these five specimens is not printed in boldface. However, by viewing the crack densities of the specimens stressed to 80, 90, and 100 percent of the C_O , a strong indication of zones of intense cracking appears. The majority of the 20-plus contours appear in bands which could be drawn from the top two corners to the center of the specimen. Figure 23 shows a well-developed failure plane commencing at the top right-hand corner and traversing into the central region of the specimen. This specimen exhibits an excellent failure plane believed to be the start of a cone break. The left side of the specimen is not a mirrow reflection of the right side as might be expected; however, a failure zone is partially developed at about 0.3 r from the platen.

Figure 30 is a composite illustrating crack-density contours of 20 and greater for all five stressed specimens just discussed. The numbers within the contour lines represent the value of stress applied to the individual specimens. The composite again shows the failure plane on the right side of the specimen. In addition, two other interesting features are revealed: one is the apparent extent of failure and the other is the presence of a minor amount of cracking in the top region of the specimen.

The approximate extent to which failure propagated (assumed extent shown by a dashed straight line) in any one specimen is apparent. The line could be shifted up or down slightly; however, it seems realistic where it is drawn in view of the fact that about 90 percent of the contour lines fall below the assumed dashed line. The approximate extent of failure along the longitudinal axis of symmetry coincides with the extent observed in the finite element models; e.g., 1.0 r to 1.5 r from the platen (see Figure 18). The solid line in Figure 30 shows the extent of failure suggested from the finite element data. Again, the theoretical and laboratory models show agreement. The extent of failure at the free boundary in the laboratory model is close to that observed in the theoretical model. The dashed line, indicative of a failure plane, is very nearly equal in slope to the slope measured on seven of the ten specimens tested for ultimate C_0 . The dashed line is inclined 55 degrees from the horizontal axis. Seven of the ten C_0 specimens developed cone breaks upon final collapse, and the average slope of the cones equaled 60 degrees. Three specimens broke with partially developed cones and axial cleavage. The average height of
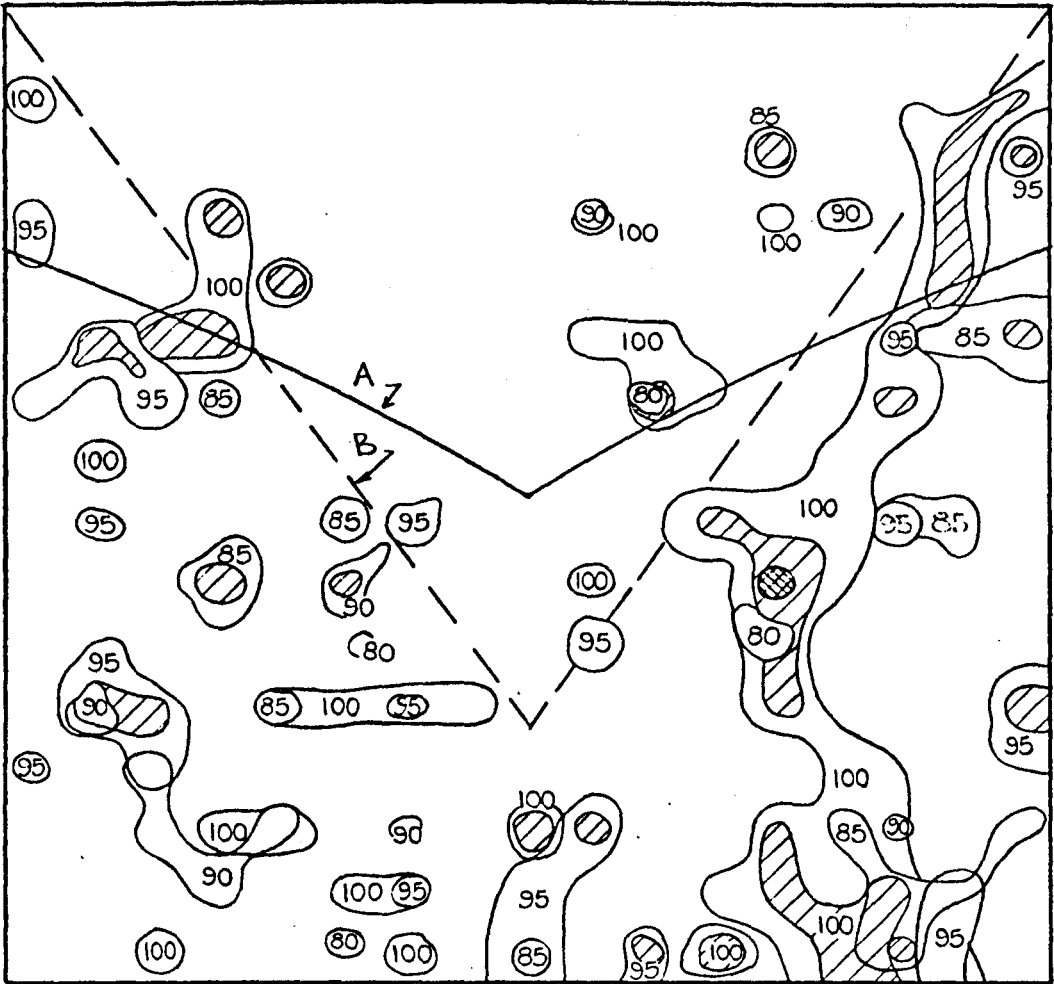
NOTE: Line A.   Extent of Failure Suggested from Finite Element   Data.
        Line B.   Assumed Extent of Failure from Laboratory Data.

Figure 30.   Composite of Crack Density Contours of 20 and
             Greater, $D_p/D_s = 1$.

the cones was 1.4 in. or about 1.5 r from the platen. Again, there is good agreement between the theoretical and laboratory models.

The small amount of cracking present above the dashed lines is most significant. Not only is there little cracking shown in the top region of the composite illustrating crack density contours of 20 and greater, but there is very little in the composite showing density contours of 15. This composite is not shown here because it was too cluttered in the mid-region. The most significant aspects of the lack of cracking above the dashed lines are: (1) it proves that end restraint due to the large elastic mismatch (steel on rock) provides high confining stresses and (2) it validates some of the predictions of the finite element code used in this study; e.g., the code predicted the approximate location where failure would propagate to within the specimen.

Figures 24-29 represent data from the test specimens which had a $D_p/D_s = 3$. The crack density contours are similar to those previously discussed. Figure 24 shows cracking starting in the central region of the specimen. This series does not readily indicate the extent to which failure propagated nor does it indicate a well-developed failure plane.

Figure 26 appears to have a partially developed failure plane on the left side of the specimen. It is believed, however, that this specimen could be an example of eccentric loading. Notice the intensity of cracking on the left side and the near absence of cracking on the right side. A low level of cracking appears in the top central region which is quite similar to the composite for $D_p/D_s = 1$ specimens.

The crack density contours of specimens receiving higher levels of stress are really somewhat nondescript. If anything, it would appear that the wider platen is causing a higher degree of cracking in the

63

central portion of the specimens. Figure 29 illustrates a greater amount of cracking in the central region and relatively little near the top corners adjacent to the platen. The extent of cracking at the free boundary for this specimen occurs about 1.0 r from the specimen top. Figure 18 shows the extent of cracking at 1.5 r for $D_p/D_s = 3$ in the theoretical model. This is not as close an agreement as has been observed previously.

Figure 31 is a composite illustrating crack density contours of 20 and greater for all six stressed specimens for $D_p/D_s = 3$. The top central region of the composite shows very little cracking, again indicating high confining stresses caused by the platen-rock elastic mismatch. A conclusive statement concerning the extent of propagation for $D_p/D_s = 3$ is not made due to the lack of crack development. A possible explanation for the low level of cracking is the range in strength for the rock. The range in C_o is 2800 psi, and some of these specimens could have been on the lower end of the strength range. If this were the case, then specimens could have developed less cracking than anticipated.

Top of Specimen

20+ ▢   25+ ▨
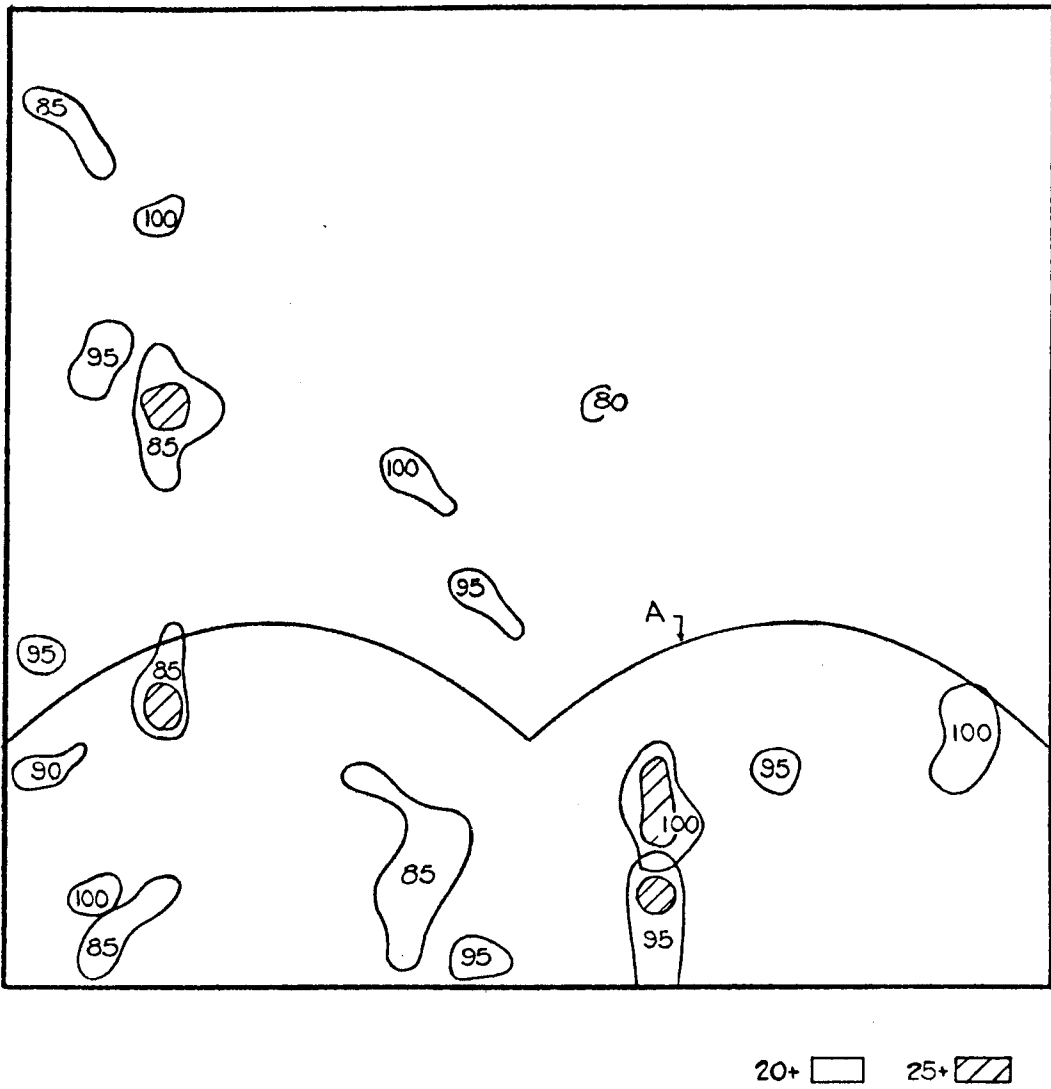
NOTE: Line A. Extent of Failure Suggested from Finite Element Data.

Figure 31. Composite of Crack Density Contours of 20 and
            Greater, $D_p/D_s = 3$.

V. SUMMARY AND CONCLUSIONS

Summation

This paper presents the results of nine theoretical and two laboratory models of an unconfined compression test on granite rock cores. A two-dimensional elastic-elastoplastic finite element code was used to simulate compression test configurations where L/D = 2, 2.5, and 3 and where D_p/D_s = 1, 2, and 3 (D_p/D_s is the ratio of the diameters of the end platen and the specimen). Three problems (one for each L/D) were run separately using the three cases (D_p/D_s). One problem (L/D = 2) and two cases (D_p/D_s = 1 and 3) were run as laboratory models. The specimen dimensions for the code and laboratory work were nearly identical, while the elastic properties of the laboratory specimens were quite similar to the elastic properties used in the theoretical models.

The theoretical models were analyzed for the influence of specimen L/D and D_p/D_s ratios upon stress trajectories, initiation of failure, and propagation and extent of failure. The laboratory specimens were stressed to various percentages of the average compressive strength. They were then sawed, and a quarter section was polished and examined for intensity of cracking under 40X magnification. A crack density scheme was utilized to plot crack density contours from which failure planes and the extent of failure were inferred. Correlations were made between the laboratory and theoretical results, and in a number of instances, good agreement was found to exist.

The results of this study together with the experimental work of others warrant the following conclusions.

Conclusions

This study has indicated fair agreement between theoretical and laboratory models for an intact granite rock loaded in unconfined compression. The parameters which show agreement and conclusions drawn from the models studied are enumerated below:

1. Length/diameter ratios from 2 to 3 have no apparent effect upon stress trajectories in the platen or specimen for $D_p/D_s = 1$, 2, and 3; however, a $D_p/D_s > 1$ has a significant effect upon stress trajectories for each of the L/D ratio studied. High shear, confining, and vertical stresses occur in areas where appreciable changes in the direction of the principal stresses exist. The stress trajectories are nearly vertical and horizontal near the free boundary at about 0.75 r from the platen for cases where $D_p/D_s = 2$ and 3.

2. Theoretical and laboratory models show that failure commences in the center of the specimen and propagates upward and outward. The extent to which the failure propagates is partially dependent upon the platen diameter and upon the elastic mismatch between platen and specimen.

3. The assumed failed zone (bounded by elastic material and a band of crushed material) for L/D = 2, $D_p/D_s = 1$ in the theoretical model, the extent to which failure propagated, is nearly identical to the observed failed zone in a duplicate laboratory model.

4. Due to the elastic mismatch and platen diameters greater than specimen diameters, a zone of complex stresses exists in the top and bottom central region of the specimen. This zone exists to a depth of 1.5 r from the platen on the longitudinal axis of symmetry. Both the theoretical and the laboratory models exhibit this zone. The zone is

bounded by a line or narrow band of intense cracking extending towards the corners of the specimen. Intersection at the free boundary is believed to be no greater than 0.5 r from the platen-specimen interface. This is the path along which cone breaks develop.

5. Due to the depth of the complex stress zone, a minimum $L/D = 2.5$ is suggested for unconfined compression testing.

6. The finite element code indicates yielding occurs at lower percentages of the input load when $D_p/D_s > 2$ for $L/D = 2.5$ and 3 . This suggests that a $1 \leq D_p/D_s \leq 2$ should be used for unconfined compression testing. A $D_p/D_s = 1$ is suggested because end restraint is considerably lower than when $D_p/D_s > 1$.

7. Shear, confining, and vertical stresses adjacent to the ends of the specimen increase with increased platen diameter.

8. The laboratory tests were inconclusive as to the final shape of the collapsed specimen. The majority of the specimens collapsed with cone breaks; however, some contained axial cleavage. It is possible that the final shape of the collapsed specimen is a function of the frictional properties of the platens.

9. The majority of observed cracks in stressed specimens were parallel to the direction of axial loading.

Suggestions for Further Research

As an outgrowth of this study, the following suggestions for further research are made:

1. Laboratory models duplicating those theoretical models not tested in the laboratory during this study should be run to further verify the code predictions.

2. Other mechanical testing configurations commonly used in the rock mechanics laboratory should be analyzed using an appropriate code. A check on the configuration of testing could lead to better methods of test and, hence, more meaningful material property data.

3. A study to determine a platen material, not necessarily a material with identical elastic properties as the specimen being tested, and a platen configuration which imparts a uniform distribution of stress throughout a material tested in compression should be undertaken.

REFERENCES

Annual Book of ASTM Standards (1971), Part II, Designation: D 2938-71
and D 2936-71, ASTM, Philadelphia, Pa., 935-936.

Argyris, J. H. (1960), Energy Theorems and Structural Analysis,
Butterworth's, London. (Reprinted from Aircraft Engineering,
Oct 1954-May 1955.)

"Basic Statistical Definitions and Procedures," (1958), Miscellaneous
Paper No. 2-250, U. S. Army Engineer Waterways Experiment Station,
Vicksburg, Miss.

Bieniawski, Z. T. (1968), "Mechanism of Brittle Fracture of Rock,"
Parts I, II, and III, Int. J. Rock Mech. Min. Sci., 4, 395-430.

Brace, W. F., and Bombolakis (1963), "A Note on Brittle Crack Growth in
Compression," J. Geop. Res., 68:12, 3709-3713.

Chugh, Y. P. (1968), "An Investigation of Frequency Spectra of Micro-
seisms Emitted from Rock Under Tension in the Range 300-15,000
cps," M.S. Thesis, The Pennsylvania State University.

Clough, R. W. (1960), "The Finite Element Method in Plane Stress
Analysis," Proceedings, Second Conference on Electronic
Computations, ASCE, Pittsburgh, Pa., Sept.

Cook, N. G. W. (1965), "The Failure of Rock," Int. J. Rock Mech. Min.
Sci., 2, 389-403.

Dahl, H. D. (1969), "A Finite Element Model for Anisotropic Yielding in
Gravity Loaded Rock," Ph.D. Thesis, The Pennsylvania State
University.

Handbook for Concrete and Cement (1949), U. S. Army Engineer Waterways
Experiment Station, CE, Vicksburg, Miss. (with quarterly
supplements).

Hardy, H. R., Jr., Kim, R. Y., and Stefanko, R. (1968), "Correlation of
Microseismic Activity and Inelastic Behavior in Geologic Materials
Under Stress," Presented at Canadian Association of Physicists
Congress, Calgary, Alberta.

Hardy, H. R., Jr., Kim, R. Y., Stefanko, R., and Wang, Y. J. (1970),
"Creep and Microseismic Activity in Geologic Materials,"
Proceedings of the Eleventh Symposium on Rock Mechanics, The
University of California, June 1969, 377-413, AIME, New York.

Hawkes, I., and Mellor, M. (1970), "Uniaxial Testing in Rock Mechanics
Laboratories," Special Issue of Engineering Geology, 4:3, 177-285.

Heard, H. D. (1968), "Effect of Large Changes in Strain Rate in the
Experimental Deformation of Yule Marble," J. of Geol., 71:2, 162.

Hetényi, M. (1950), Handbook of Experimental Stress Analysis, New York, John Wiley & Sons.

Hsu, Thomas T. C., Slate, F. O., Sturman, G. M., and Winter, George (1963), "Microcracking of Plain Concrete and the Shape of the Stress-Strain Curve," American Concrete Institute, 60:2, 209-223.

Layne, Abner A., Ed. (1969), "Materials Selector Issue," Materials Engineering, 70:5, 1-515, Mid-Oct.

Paulding, B. W., Jr. (1965), "Crack Growth During Brittle Fracture in Compression," Ph.D. Thesis, Massachusetts Institute of Technology.

Peng, S., and Johnson, A. M. (1972), "Crack Growth and Faulting in Cylindrical Specimens of Chelmsford Granite," Int. J. Rock Mech. Min. Sci., 9:1, 37-86.

Saucier, K. L., and Ainsworth, D. L. (1969), "Tests of Rock Core, Warren Study Area, Wyoming," Miscellaneous Paper C-69-3, U. S. Army Engineer Waterways Experiment Station, Vicksburg, Miss.

Scholz, C. H. (1968), "Experimental Study of the Fracturing Process in Brittle Rock," J. Geop. Res., 73:4, 1447-1454.

Stowe, R. L. (1967), "Development of a Microcracking Technique for Measuring In-Situ Stress and Strain," Report 1, Technical Report No. 6-764, U. S. Army Engineer Waterways Experiment Station, Vicksburg, Miss.

Stowe, R. L. (1969), "Stress Distribution in Cylindrical Test Specimens Under Uniaxial Load," Internal Report RML-IR/69-15, Dept. of Mining, The Pennsylvania State University.

Walsh, J. B. (1965), "The Effect of Cracks on the Compressibility of Rock," J. Geop. Res., 70:2, 399-411.

Willard, R. J., and McWilliams, J. R. (1969), "Microstructural Techniques in the Study of Physical Properties of Rock," Int. J. Rock Mech. Min. Sci., 6:1, 1-12.

Zienkiewicz, O. C., and Cheung, Y. K. (1967), The Finite Element Method in Structural and Continuum Mechanics, London, McGraw-Hill.

DOCUMENT CONTROL DATA - R & D

(Security classification of title, body of abstract and indexing annotation must be entered when the overall report is classified)

1. ORIGINATING ACTIVITY *(Corporate author)*	2a. REPORT SECURITY CLASSIFICATION
U. S. Army Engineer Waterways Experiment Station Vicksburg, Mississippi	Unclassified
	2b. GROUP

3. REPORT TITLE

PROPAGATION OF FAILURE IN A CIRCULAR CYLINDER OF ROCK SUBJECTED TO A COMPRESSIVE FORCE

4. DESCRIPTIVE NOTES *(Type of report and inclusive dates)*
Final report

5. AUTHOR(S) *(First name, middle initial, last name)*

Richard L. Stowe

6. REPORT DATE	7a. TOTAL NO. OF PAGES	7b. NO. OF REFS
December 1973	78	26

8a. CONTRACT OR GRANT NO.	9a. ORIGINATOR'S REPORT NUMBER(S)
b. PROJECT NO. 4A061101A91D	Miscellaneous Paper C-73-12
c. Task 02, Work Unit 040	9b. OTHER REPORT NO(S) *(Any other numbers that may be assigned this report)*
d.	

10. DISTRIBUTION STATEMENT

Approved for public release; distribution unlimited.

11. SUPPLEMENTARY NOTES	12. SPONSORING MILITARY ACTIVITY
	Assistant Secretary of the Army (R&D) Department of the Army Washington, D. C.

13. ABSTRACT

This study was designed to contribute to our understanding of how well an intact rock can be modeled using a theoretical model and laboratory tests of the same model. An elastic-elastoplastic finite element code was used to analyze the failure growth of intact rock specimens subjected to uniaxial compression. Intact rock specimens with the same dimensions, test configurations, and physical properties as the finite element model were tested in the laboratory and examined for failure zones and the propagation of failure. Theoretical and laboratory models show that failure commences in the center of the specimen and propagates upward and outward. The extent to which the failure propagates is partially dependent upon the platen diameter and upon the elastic mismatch between platen and specimen. Results of the finite element and laboratory models compare quite favorably, i.e., model simulation reasonably predicted the failure characteristics of an actual model. Both models show that failure commences in the center of the model and propagates upward and outward until a free boundary is encountered. Test results suggest that a minimum $L/D = 2.5$ and a $1 = D_p/D_s \leq 2$ be used for unconfined compression testing of cylindrical rock specimens.

DD FORM 1473 REPLACES DD FORM 1473, 1 JAN 64, WHICH IS OBSOLETE FOR ARMY USE.

Unclassified
Security Classification

14. KEY WORDS	LINK A		LINK B		LINK C	
	ROLE	WT	ROLE	WT	ROLE	WT
Finite element model						
Igneous rock						
Rock failure						
Rock mechanics						
Uniaxial compression						

In accordance with ER 70-2-3, paragraph 6c(1)(b),
dated 15 February 1973, a facsimile catalog card
in Library of Congress format is reproduced below.